NASA Technical Memorandum 100872

Techniques Utilized in the Simulated Altitude Testing of a 2D-CD Vectoring and Reversing Nozzle

H. Bruce Block, Lively Bryant, John H. Dicus, Allan S. Moore, Maureen E. Burns, Robert F. Solomon, and Irving Sheer
Lewis Research Center
Cleveland, Ohio

June 1988

NASA

TECHNIQUES UTILIZED IN THE SIMULATED ALTITUDE TESTING OF A 2D-CD VECTORING AND REVERSING NOZZLE

H. Bruce Block, Lively Bryant, John H. Dicus, Allan S. Moore,
Maureen E. Burns, Robert F. Solomon, and Irving Sheer
National Aeronautics and Space Administration
Lewis Research Center
Cleveland, Ohio 44135

E-4096

SUMMARY

Simulated altitude testing of a two-dimensional, convergent-divergent, thrust vectoring and reversing exhaust nozzle was accomplished at NASA Lewis Research Center. Research objectives included the measurement of nozzle and reverser performance, nozzle liner material durability, and the transient behavior of the engine and nozzle combination over a wide range of operating conditions. Another important objective was to develop test hardware and techniques to properly operate a vectoring and reversing nozzle within the confines of an altitude test facility. This report presents detailed information on the major test support systems utilized, the operational performance of the systems and the problems encountered, and test equipment improvements recommended for future tests. The most challenging support systems included the multi-axis thrust measurement system, vectored and reverse exhaust gas collection systems, and infrared temperature measurement systems used to evaluate and monitor the nozzle.

All project research objectives were accomplished, and the feasibility of testing a vectoring and reversing nozzle of this type in an altitude chamber was successfully demonstrated. Supporting systems performed as required. During reverser operation, the engine exhaust gases were successfully captured and turned downstream. However, a small amount of exhaust gas spillage out of the collector ducts' inlet openings occurred when the reverser was opened more than 60 percent. The spillage did not affect engine or nozzle performance. The three infrared systems which viewed the nozzle through the exhaust collection system worked remarkably well considering the harsh environment. All required temperature data were obtained.

INTRODUCTION

Simulated altitude testing of a two-dimensional, convergent-divergent (2D-CD), vectoring and reversing exhaust nozzle on an advanced F100 derivative engine was accomplished at NASA Lewis Research Center in the Propulsion Systems Laboratory. Major test objectives included the determination of 2D-CD nozzle aerodynamic performance and cooling system effectiveness, determination of nozzle liner material durability, thrust reverser performance, and a study of the transient behavior of the engine and nozzle combination during vectored and reverse operation. Another important objective was to develop test hardware and techniques to properly operate a thrust vectoring and reversing nozzle within the confines of an altitude test facility. During test operations, the engine was operated over a wide range of power settings up to maximum power,

altitude was varied between 3050 m (10 000 ft) and 12 190 m (40 000 ft), the nozzle was vectored between 0° and 20° and the reverser was operated between 0 and 100 percent open.

At the point in time when this test was completed (March 1986), the facility capability developed for this project was unique within the U.S. The most important special consideration was the design of systems to collect vectored and reversed exhaust gases. In addition, special instrumentation systems were developed to measure multi-axis thrust, and to determine the internal and external surface temperatures of the 2D-CD nozzle. The multi-axis thrust system measured axial, lateral, and vertical thrust components. Nozzle surface temperatures were measured using five infrared (IR) systems.

In order to share the test hardware details and techniques developed at NASA Lewis with other interested parties, this report presents detailed discussions of the following major test support systems: inlet air ducting and flow measurement hardware; engine and nozzle installation; multi-axis thrust measurement system; vectored and reverse exhaust gas collection systems; and the infrared temperature measurement system. In addition, operational problems and recommended solutions are discussed.

APPARATUS AND METHODS

Test Facility

The Propulsion Systems Laboratory consists of two altitude test chambers connected to a central combustion air and altitude exhaust system (fig. 1). The test chambers are capable of testing full-scale airbreathing and rocket engine systems under controlled, simulated flight conditions. Airbreathing engines are tested in the direct connect mode. Since test activities began in 1973, the Propulsion Systems Laboratory has completed numerous research and development projects studying all the significant aspects of jet engine system technology.

The test chambers are 11.6 m (38 ft) in length and 7.3 m (24 ft) in diameter. Figure 2 shows the overall layout of this facility. System capabilities are also presented including maximum air flow, inlet air temperature range and altitude range. Figure 3 presents a cutaway view of the Propulsion Systems Laboratory showing the relative locations of the test chambers, the Control Room, and the Data Preparation Room.

The steady-state data system can process over 1200 test measurements per second providing data recording, output displays, limit checking, and some control functions. Analog and digital data recording systems are also available to support transient test activities.

Project and Installation General Description

The research project was a joint program between NASA, the U.S. Air Force and Pratt & Whitney Aircraft to test a full scale, two-dimensional convergent-divergent (2D-CD), vectoring and reversing exhaust nozzle on an advanced F100 derivative engine at simulated altitude conditions. Test objectives included measurement of nozzle internal aerodynamic performance and cooling system

effectiveness, determination of nozzle liner durability, thrust vectoring and reverser performance, and an evaluation of engine/nozzle operability during steady state and transient operation. Because this type of testing had not been previously accomplished in an altitude facility, another important objective was the development of test hardware and techniques to successfully operate a vectoring and reversing nozzle within the confines of an altitude facility.

The engine used in this project was a Pratt & Whitney Aircraft PW1128, which is a derivative of the F100 engine. The 2D-CD nozzle was a research configuration, constructed to simulate the internal flow of a flight-type nozzle, but containing nonflight weight external structural components. The nozzle was capable of producing axial and vectored thrust from idle to maximum afterburning power settings. Nozzle reverse thrust capability was limited to between idle and intermediate power settings. Vectored exhaust gas temperature exceeded 1922 K (3000 °F), while reverse exhaust gas temperature was a maximum of 866 K (1100 °F). The engine and nozzle were controlled by separate digital electronic controllers which were interfaced to operate as a unit.

Figure 4 shows the overall installation of this project in test chamber 3 of the Propulsion Systems Laboratory. The configuration shown is for the vectored nozzle tests, but is representative of the general layout of required equipment. From the left side of figure 4, conditioned air from the facility inlet section entered a bellmouth (not visible), flowed through the inlet ducting and entered the engine. Exhaust exited the nozzle and was captured in the exhaust collection system. The inlet ducting contained an air flow measurement station, a metric break, engine inlet instrumentation and several supports. The engine and nozzle were mounted in a thrust measurement system which was capable of measuring forces in the axial, lateral, and vertical directions. The exhaust collection system contained three viewports to enable IR monitoring of nozzle internal surface temperatures. Two other infrared systems were used to monitor nozzle external temperatures.

During operation, the test chamber hatch was closed and the internal pressure was controlled to a sub-atmospheric level to simulate the desired altitude. The chamber was maintained below 65 °C (150 °F) during testing using cooling air from a torus. Cooling air was supplied at ambient temperature and a nominal flow rate of 22.7 kg/s (50 lbm/sec). Color television systems were used to monitor test equipment in the chamber after the hatch was closed.

The following sections describe each of the major test components in detail.

Inlet Ducting System

Conditioned inlet air was directed from the plenum chamber through a bellmouth and air flow measurement station (station 1). The inlet mass flow rate to the engine was determined at this station by the method described in appendix A and reference 1. Downstream of the flow measurement station (fig. 4), the inlet duct was anchored to the test chamber floor (ground).

The inlet section between the anchor point and the engine inlet flange contained the inlet seal assembly, engine inlet instrumentation section (station 2), and an articulated duct (fig. 5). The articulated duct has a double

gimbal arrangement which allowed the duct section to move radially in response to any engine inlet flange motion or deflection. This duct section was counterbalanced with a spring hanger assembly in order to minimize shear and bending loads on the engine inlet flange (null load pickup point in fig. 8). A vertical load cell was installed in line with the spring hanger assembly to measure any gimbal friction loads which could influence vertical thrust measurements.

The inlet seal system used an inflatable silicone rubber torus. The seal was retained to the duct assembly, and the engine inlet instrumentation spool piece telescoped through the inside diameter of the seal. This arrangement accommodated axial thermal growth, axial system deflections, and provided a thrust metric break. The seal also provided accommodation for small angular misalignment. The seal pressure was maintained at a positive constant pressure as referenced to inlet duct static pressure using a specially adapted pressure regulator. The point of contact between the inflatable seal and the inlet instrumentation spool piece was defined as the thrust metric break (fig. 5). This particular seal configuration was designed for a 27.6 N/cm^2 (40 psid), 433 K (320 °F) environment and has a long history of satisfactory operation. The seal mating surface was polished and silicon dry lubricant was applied to minimize seal drag.

Engine and Nozzle Installation

The 2D-CD nozzle was directly attached to the engine at the standard attachment interface referred to as the "K" flange. An unreinforced aft fan duct case was used on the engine, thus certain test conditions were eliminated due to the potential for high case stresses. The engine was mounted to the thrust measurement system using the standard rear thrust mount points and the forward link attachment point (fig. 6). Specific engine mounting details are discussed in the next section. The center of gravity of the engine and nozzle assembly was aft of the engine rear thrust mount plane.

Engine case bending stresses resulting from the nozzle dead weight load were within an acceptable range. However, nozzle vertical thrust operation was restricted to the upward direction (vector down) operating mode. Operation in the vertical thrust down mode (vector up) would have caused unacceptable engine aft fan duct bending stresses. Also, nozzle "blowoff" loads resulting from full reverse thrust at high dynamic pressure conditions would have resulted in tensile overstress of the engine structure and were thus avoided.

The convergent and divergent nozzle panels, and the nozzle stationary sidewalls had removable liner inserts. These liners shielded the nozzle structure from the exhaust gases and were internally air cooled. Seals were installed at the convergent/divergent panel hinge lines and at contact lines between the panels and the stationary walls. Cooling air was supplied from the engine fan bypass duct and facility sources. Cooling air flow rates were measured as were a number of nozzle pressures and temperatures.

Engine inlet pressure and temperature were measured at the station 2 spool just upstream of the engine and at the leading edge of the engine inlet-guidevanes (using a number of small sensors located within the vanes).

Fuel, hydraulic, and cooling air lines to the engine and nozzle crossed the thrust metric break in a flexible manner and were routed perpendicular to the axial thrust measurement axis. Instrumentation lines were looped in such a way as to minimize thrust drag forces.

Multi-Axis Thrust Measurement System

One of the requirements of this project was to determine the gross thrust of the engine and nozzle assembly. The axial and vertical components were the primary items of interest even though lateral thrust was also measured. Determination of axial gross thrust required accurate determination of measured forces, engine inlet flow momentum, static pressure forces, and installation drag forces. Likewise, determination of vertical gross thrust required accurate determination of measured forces and static pressure forces. The derivation of the gross thrust equations is further discussed in appendix B.

The thrust measurement system used for this project contained elements to measure axial, lateral, and vertical thrust (Fa, Fh, and Fv respectively) and to measure pitch, roll, and yaw moments (Mp, Mr, and My respectively). However, the system was only equipped to calibrate the three thrust forces and one moment (yaw). The system can be mechanically described as follows: a core axial/lateral thrust measurement package used for a previous project (ref. 2); and an engine mount system which was modified to include vertical thrust measurement elements. The thrust measurement system was calibrated for in-stand interactions and external drag loads.

Axial and lateral thrust measurement. - This portion of the thrust measurement system was designed and fabricated as a package by Ormond, Inc. (ref. 3). It was mounted to the test cell floor using a three point suspension adaptation structure (fig. 7). This structure served to isolate any facility test bed bending or torsional stresses and deflections from the thrust measurement system. The structure which cradles the engine and nozzle and vertical thrust measurement system was mounted on the top side of the axial/lateral thrust package. The package consisted of an upper (live or metric) table with both lateral and axial calibration load cell trains and a lower (fixed or ground) table with both lateral and axial measurement load cell trains (fig. 8). The upper table was supported from the lower table by a set of eight flexural links, two at each corner of the table. Each corner pair consisted of one flexural link in tension and one flexural link in compression.

The horizontal axes of the axial and lateral load cells were in the same plane, with the lateral axes mutually perpendicular to the axial axis. Likewise, the same conditions held true for the calibration system load cells. The horizontal planes of both load cell systems were parallel to each other and the engine axial centerline. The engine axial centerline and the axial measurement and calibration load cell centerlines were aligned into the same vertical plane. Two lateral load cell locations were used, one at the forward end of the thrust measurement system and the other at the aft end. The complementary calibration load cells were located in the same vertical planes as their respective data measurement load cells.

All load cells in this system were installed with universal flexures at each end of the load cells. These flexures provided axial stiffness with no axial motion and provided limited angular flexibility. This system minimized

the effect of side loads on the load cells from such sources as minor misalignments and from off-axis thrust loads.

The axial measurement load cells were arranged in tandem, with one in tension and the other in compression when an axial load was applied. The arithmetic sum of the two load cell readings represented the indicated axial thrust. The complementary axial calibration load cell train was similarly arranged. A synchronized hydraulic motor driven jackscrew system applied bidirectional axial loads to the calibration load cell train (forward or reverse thrust). Single load cells were used for lateral measurements. The algebraic sum of forward and aft load cells represented the indicated lateral thrust. The yaw moment was also resolved from these two load cell readings. Bidirectional loads were applied to the complementary calibration load cells at each lateral location. The lateral calibration loading system also used hydraulic motor driven jackscrews.

When the thrust system was operational, the calibration loading system was decoupled from the system through use of stable platen assemblies (hinged plate structures, fig. 8). When a calibration load was applied to the calibration load cell train, the stable platen deflected axially with the applied load. When the loading device was retracted to a neutral position, the platen also reached its neutral position. The platen had a low spring rate in the direction of the applied load. Consequently, when the affected load cell train was relaxed, only a minimum tare reaction was seen in the measured load cell readings.

Vertical thrust measurement. - The engine/nozzle assembly and the vertical thrust measurement system were mounted to an engine mount-adapter structure, which in turn was mounted on the top side of the axial/lateral thrust measurement system (fig. 9). Three load cells were used for the vertical measurement. Two units were located in the axial plane of the rear thrust mounts and the third unit was mounted vertically in line with the forward attachment link. The algebraic sum of the indicated forces represented the vertical thrust component resulting from vectoring the nozzle.

The rear engine thrust mounts were engaged in a yoke assembly which encircled the engine at this axial location (figs. 10(a) and 10(b)). The yoke rested on two symmetrically placed load cells which measured the vertical forces at this location. The load cells had universal flexures installed on each end. The yoke was stabilized in the vertical position by three hinge plates which were anchored to the mount structure. Rigidity was provided in the axial and lateral planes, while flexibility was retained in the vertical direction. The lateral rear stabilizer link was attached to the yoke assembly and to the engine. The stabilizer link was used to maintain the engine lateral centerline location.

The forward engine mount point was attached to the mount structure through use of a vertical link assembly (fig. 11). This assembly contained the measurement load cell and one universal flexure.

Vertical measurement load cells were calibrated in place using two symmetrically placed calibration fixtures which were installed external to the thrust measurement system. These fixtures applied a vertical upward load on each side of the nozzle (fig. 9). The calibration loads were applied with pneumatic

linear actuators and were measured with single load cells on each side. The actuators and load cells were retracted when not in use.

A bolt and bracket arrangement attached to the vertical calibrate fixtures provided adjustable nozzle stops to limit nozzle upward travel when operating in the vectored mode. A contact warning system was provided.

Multi-axis thrust calibration procedures. - Before proceeding with the 2D-CD project tests, three calibration procedures were required for the multi-axis thrust stand. The first of these procedures determined first-order, in-stand interactions (as described in appendix B) between axial, lateral, and vertical loads (second-order effects were assumed to be negligible). Calibration loads were independently applied at each calibration location (axial, forward lateral, aft lateral, and vertical) and the effects on all measuring load cells were recorded. This calibration matrix was conducted at atmospheric conditions and at a test cell pressure of 3.4 N/cm^2 (5 psia). Load cell interaction coefficients were determined from this information. The interaction coefficients were used to correct the measured load cell readings in determining actual loads applied to the thrust stand during test operations. No altitude effects were observed with respect to the interaction coefficients.

The second calibration test was made to determine the effective engine inlet seal force (at the metric break). This was done by determining the effective area of the seal at static conditions (engine not operating). For this test, the engine inlet instrumentation spool piece was mounted to a blank-off plate, which in turn was anchored to the engine mount-adapter (fig. 12). The inlet seal was set up in its normal mode with respect to the inlet spool piece (a short section of inlet ducting was removed for this test). By varying the inlet and test cell pressures on each side of the blank-off plate, a range of ram ratios corresponding to engine operating envelope conditions was duplicated. The seal pressure was maintained at a positive constant pressure as referenced to inlet pressure. The pressure loads were transmitted to the multi-axis thrust stand. The effective seal area was determined using the measured axial load forces, and seal and test cell static pressures. This area was used in the axial gross thrust determination.

The third calibration test required was to determine drag forces due to test cell cooling air impinging on the engine and thrust measurement installation. For this test, all systems were in the mechanical configuration used for test operations. All electrical and instrumentation lines were in place and all support systems were pressurized (where applicable). With no inlet air flow and the engine locked from rotation, a matrix of cell cooling air flows and altitudes (cell static pressure) were run. This matrix corresponded to the expected test program ranges. The drag forces were transmitted to the thrust system and measured with the axial load cells. This drag force calibration data was incorporated into the axial gross thrust determination.

Exhaust Collection System for Vectored Operation

Design criteria. - Capture of exhaust gases at high temperatures and over a wide range of operating conditions was required. As discussed previously, the nozzle operated between 0° and 20° downward vector angles. Power settings ranged from idle to maximum afterburner, while inlet and exhaust conditions were varied to cover most of the engine normal operating range. Engine

airflows over 90.7 kg/sec (200 lb/sec) were expected along with a nominal cell cooling airflow of about 22.7 kg/sec (50 lb/sec). Nozzle exhaust gas core temperature was estimated to be over 1922 K (3000 °F). Desired exhaust collector characteristics included: long operational life without failure (1000+ hr withstanding the expected thermal and mechanical loads); the ability to minimize recirculation of exhaust gases back into the test chamber; and provision for mounting three viewing ports which the infrared cameras used to monitor nozzle internal surface temperatures. Cooling tower water was available in the test chamber for the exhaust collector at a supply pressure of 29 N/cm^2 (42 psig) and a return pressure of 3.4 N/cm^2 (5 psig). Previous experience at the Propulsion Systems Laboratory indicated the following: air temperature inside the collector, about 0.15 cm (0.06 in.) from the inner wall surface, should not exceed 1172 K (1650 °F) when the nozzle was vectored 20° downward; an overall heat transfer coefficient from the exhaust gas to the collector wall (including radiation and convection heat transfer) of about 1136 W/m^2 C (200 BTU/hr-ft^2-°F) in the region where the exhaust plume intersected the collector wall was anticipated; and the maximum allowable collector metal surface temperature in contact with the cooling water was limited to 422 K (300 °F).

Design and installation details. - A configuration using two water cooled exhaust collector spools was selected (fig. 13). The center line of the collectors was offset 20.3 cm (8 in.) below the center line of the engine to provide a location for mounting the infrared camera windows out of the exhaust plume (while enhancing the view of the nozzle), to provide a larger capture area for the vectored plume below the engine center line, and to spread the plume heat load over a larger area. An air manifold was installed at the inlet end of the collector on the adapter plate to supplement cooling of the lower half of the collector where the heat load was most severe (fig. 14).

Three window ports were positioned at discrete locations around the collector to provide the optimum view of the nozzle (given the 30° by 60° rectangular field of view of the IR camera) while keeping the camera lens forward of the exhaust plume. By drawing a scaled layout of the nozzle, collector, and camera windows, a determination was made of the optimum locations for each window covering the full range of expected nozzle positions. Figures 13 and 15 show the window locations on the forward collector and the areas inside the nozzle which could be seen during various nozzle and engine operating modes. Figure 16 shows a detail of he IR camera window installation as initially installed. Each window port was provided with a bellows to allow for differences in expansion between the water cooled inner and outer shells. Each window housing had an external water inlet and outlet port to ensure that water circulation through the collector did not bypass the window housings. Various sapphire window sizes were used throughout the project. A 16.5 cm (6.5 in.) diameter window size was initially selected to enable maximum viewing. A window thickness of 0.94 cm (0.37 in.) was selected to withstand a maximum differential pressure of 3.4 N/cm^2 (5 psid). The windows had an IR spectral transmission wavelength range of 2.0 to 5.6 μm band, random orientation and 80 to 50 optical polished faces. Provisions were made to bring shop air to cool the inside surface of the windows and to air wash the same surface thus minimizing the accumulation of exhaust gas particles on the sapphire. Particles on the viewing surface could affect the IR transmission characteristics. Each sapphire window was sandwiched between two flat neoprene gaskets and assembled into an adapter ring with a cushioning "O" ring around the circumference of the window. Compression of the gaskets was controlled with shims, so the window could float within the adapter ring as the ring size changed with temperature.

Details of a basic exhaust collector spool design are shown in figure 17. Window attachment details are not shown here for simplicity. These spools had a long history of successful operation in nonvectored engine tests. Their design was conservative, and calculations indicated they would be adequate for this application. The stainless steel inside wall provided a relatively poor conductivity, thus establishing a large temperature drop which allowed the surface adjacent to the water passage to run cooler than 422 K (300 °F). The cooling water flow path provided a high cooling rate (about 5680+ W/m^2 °C (1000+ Btu/hr-ft^2-°F)), while the required water flow was within the capabilities of the supply system (about 1.2 m^3/min (320 gpm) per each collector spool).

Figure 18 shows a view of the forward collector spool installed in the test chamber. Two IR window housings can be seen. Due to the expected nonsymmetric loads on the collectors, four heavy support rods were installed at the forward end of the assembly and additional supports were added to the rear. The forward support rods were spaced about 90° apart. One of the rods is seen in figure 18.

Exhaust Collection System for Reverse Operation

Design criteria. - Capture of reversed exhaust gases was required without affecting engine/nozzle operation and without recirculation of exhaust gases into the test chamber or onto the external surfaces of the nozzle. With this configuration, the nozzle was capable of operating from 0 to 100 percent reverse, and/or 0° to 20° vectored downward in a nonafterburning mode. As afterburning was not planned to be used during reverse operations, maximum expected exhaust gas temperature was 866 K (1100 °F). Maximum reverser design values were estimated as follows: 40 034 N (9000 lbf) reverse thrust; 45.4 kg/s (100 lb/sec) flow per reverser collector duct; and a conservative 17.2 N/cm^2 (25 psid) internal differential pressure in portions of each reverser collector duct.

Another important consideration was the limited available space in the test chamber for the lower reverser duct. The test chamber floor below, the thrust measurement system forward, and the exhaust collection system aft all presented potential interferences. Long reverser duct life was not required as the ducts were considered test specific hardware. A relatively inexpensive stainless steel material was planned for the reverser ducts.

Design and installation details. - The reverser exhaust gas collection system selected is shown in figure 19. The system consisted of two uncooled reverser collector ducts, an uncooled stainless steel conical adapter, and one water cooled exhaust collector spool previously used during the vectored testing. No internal IR measurements were made during the reverser testing. The entire assembly was installed on the engine centerline. Figure 20 shows the engine, nozzle, and reverser collector ducts installed in the test chamber. Figure 21 presents a close-up view of the nozzle, reverser collector ducts, and the conical adapter. The heavy structure required to support the reverser collector ducts over a wide range of applied loads is also shown in figure 21. In addition, finger seals installed between the reverser collector ducts and upstream surface of the conical adapter are seen in this view.

The internal flow path of the reverser collector ducts was critical for proper operation. The design incorporated a series of vanes, with the first vane cascade intended to shock the flow down from a supersonic condition to a subsonic condition (fig. 22). The remaining vanes were placed to assist in turning the flow while providing a uniform flow distribution and minimizing the pressure loss. The individual vanes were attached to aerodynamically shaped vertical support bars to provide rigidity and internal support for the expected pressure loads. In the downstream portion of the reverser ducts, round support rods were installed horizontally and vertically to carry the internal pressure loads. A simplified computational fluid mechanics computer code was used to check and refine the duct shape and vane locations within the ducts. Internal pressure and temperature instrumentation was installed on the vanes and walls of each duct.

A thin walled design was selected to allow duct flexibility, thus minimizing the buildup of excessive stresses. A 0.48 cm (3/16 in.) thick 316 stainless steel was chosen for the ducts. About 5 cm (2 in.) of foil wrapped Fibrefrax insulation was applied to the exterior of each duct to prevent heat loss to the test chamber and to minimize duct thermal shock during reverser transients. During testing, the reverser was opened a small amount to allow the ducts to warm up prior to rapid transient operations.

Figure 23 shows the reverser collector ducts mounting system. The upstream end of each duct was fixed to the support structure. The downstream end was restrained in a sliding mount which allowed for axial and vertical growth. The ducts were positioned near the reverser discharge ports of the nozzle, but at no time did they contact the ports. About 1.9 cm (3/4 in.) maximum clearance was set up between the nozzle ports and the ducts. The gap was used to provide a positive metric break, thus enhancing thrust measurement. Finger seals were used on the downstream end of the reverser collector ducts at the joint with the conical adapter. This seal was thought to help minimize exhaust gas recirculation back into the test chamber.

Nozzle control cables and instrumentation were protected with metal shields and cooling air to prevent damage due to exhaust gas recirculation. External thermocouples were installed near the reverser collector duct ports to detect if hot exhaust gases were escaping from the ports.

For a more detailed description of the reverser collector duct design and an indepth assessment of its operation and performance, see reference 4.

Instrumentation

Turbine engine instrumentation. - Conventional engine instrumentation was selected for this project. Various pressures and temperatures within the engine and in the engine inlet system were measured. In addition, engine speeds, fuel flow, vibrations, thrusts, and case stresses were measured. Specific discussion of measurements are contained in appropriate sections of this report along with the hardware descriptions. Figure 24 presents the engine instrumentation stations. Nozzle internal temperature measurement is discussed below. The two IR systems used to monitor external nozzle temperatures are not discussed.

Infrared system description. - For this project it was necessary to determine temperatures and observe thermal patterns over a large temperature range, across a large nozzle surface area, through a hostile environment (jet exhaust), and on a material which would be compromised by the attachment of thermocouples (nonmetallic nozzle flaps and sidewall liners). Thus, in order to accomplish the project objectives, the noncontact method of infrared thermography was chosen. Several very good systems were available, and after evaluation, the Probeye system manufactured by Hughes Industrial Products Division was selected. The Probeye, which employs a spinning mirror scanning mechanism and Indium Antimonide (InSb) detector, is sensitive in the 2 to 5.6 μm wavelength range of the electromagnetic spectrum. This range is one of the two ranges which the atmosphere exhibits extremely good transmissive qualities to infrared energy.

To adequately monitor the engine nozzle internal surfaces, three IR systems were procured. Figure 25 presents a typical IR system configuration.

The infrared viewer contains a 10 sided rotating prismatic mirror, 6 InSb detectors, 6 light emitting diodes and associated optical and electronic hardware. The object to be viewed is placed in the optical path of the system. Infrared energy entering the viewer is scanned by the system's rotating mirror assembly. A 4.8 μm bandpass notch filter (flame filter) was used in each viewer to eliminate H_2O and CO_2 emission bands of the engine exhaust. The system specifications are as follows:

Camera environment, C	10 to 40
Spectral range, μm	2 to 5.6
Scan rate, frames/sec	20
Focus range, cm	10 to infinity
Spatial resolution, deg	0.126 horizontal and vertical
Field of view, deg	60 by 30 with wide angle lens
Line rate, lines/sec	1200
Display resolution, lines	60 per frame, interpolated to 120, converted to 300 on the monitor

Processing of raw analog data occurs in the electronic processor unit. The processor, using an analog to digital converter, creates a 16 level grey scale (4 bit resolution), with each level representing a range of thermal units. These thermal units are converted to temperatures by way of "temperature look-up tables" within the processor electronics. The face of the processor contains a keyboard of preprogrammed user-selectable function keys, and a small 7.6 cm (3 in.) color monitor which displays a color enhanced thermal image of the field of view. The keys on the processor can be described as either input functions (describing the target and environment to the system), or output functions (describing display characteristics).

Two types of output are accessible from the processor, standard color video (NTSC) and digital. To record the video signal, a VHS format video recorder was purchased with each system. The output of the recorder was viewed on each of the three monitors at different locations in the facility. To record the digital signal, a computer interface unit allowed the processor to converse with an IBM PC-AT. The recording of digital data was accomplished at the request of the IR data engineer. When a request was made, the current data displayed by the processor was captured as a single frame (or snapshot)

and transmitted to the PC via an IEEE-488 interface. The first data transmitted was reference information to coordinate the data transfer. The next data transmitted were the 60 lines of pixel data. Then a string of parameters including minimum temperature, sensitivity, emissivity, and ambient temperature were transmitted. The PC, using Hughes software and specially developed NASA software, stored the digital information on a floppy disk. The software provided the capability to view data previously recorded and to perform some post-test analysis on the data. Two of the three IR cameras' data could be recorded at one time as two PC systems were available.

Infrared system installation and operation. - The scanners were located inside the test cell, about 45.7 m (150 ft) from the control room. The IR detector array of the Probeye system, as with most IR imaging systems, required cooling to achieve cryogenic operating temperatures for the detectors. Hughes employs high pressure Argon expanded through a cryostat to cool the detectors to 86 K (-305 °F). An Argon supply system was developed using a 1517 N/cm^2 (2200 psi) bottle of Argon mounted outside the test cell and connected to a manifold which penetrated into the test cell. To insure normal operation of the scanners, it was imperative that the Argon purity specifications be met, that is, the Argon had to be pre-purified with a minimum purity of 99.998 percent and a maximum dew point of 213 K (-76 °F). A fine mesh bronze filter and a desiccant were placed in the supply tubing upstream of the scanners. Any trace moisture in the system could freeze and plug the cryostat. In addition, specific procedures were defined for cleaning, purging, and evacuating the supply lines.

After extensive evaluation of axial distances,viewing angles, and nozzle positions, three circumferential locations were chosen to afford the optimum view of the nozzle surfaces (figs. 13 and 15). At each location, a port was cut in the exhaust collector; a scanner, housed in a protective enclosure, was installed at each port. A sapphire window, which displays very good transmissive qualities in both the infrared and visible spectrum, was placed in the port to allow radiation to pass through while protecting the scanner from the harsh exhaust environment. Further details of this installation are covered in the exhaust collection system section of this report.

The scanner mounts were designed to anchor the scanners to a fixed position in the test chamber while still allowing for finer aiming adjustments. To determine the final position, the nozzle and other surfaces in the field of view were outlined with "heat tape" which, when activated, reached a temperature of about 316 K (110 °F). The scanners were turned on, and the thermal image of the heat tape outline allowed them to be aimed to capture the area of greatest interest. This method worked exceptionally well.

In order to determine the accuracy of the temperature readings obtained with the IR system, a reference target was constructed and fixed in the field of view of two scanners. The reference was a piece of material identical to the material lining the nozzle, instrumented with two thermocouples in such a way that the surface temperature was measured as accurately as possible. The reference was attached to the trailing edge of the nozzle sidewall so that its surface was heated by the exhaust gas exactly as the sidewall was heated. Assuming that the two surfaces were indeed heated identically, and that the thermocouples were accurate, direct comparison of the thermocouple readings and the infrared systems allowed a determination of the accuracy of the system.

The three cameras were installed within the test chamber in air cooled enclosures. Figure 26 presents a typical enclosure. Each enclosure contained a double set of vibration damping platforms and an internal liner of acoustic absorption material. Air cooling was accomplished using an expansion cooling device attached to the compressed air supply. The infrared camera components were maintained between the required temperatures. Each enclosure was supported and positioned by a unique mounting stand which allowed for fine adjustment in all planes (fig. 26). A rubber boot was used at each location to join the enclosure and the window thus maintaining vibration isolation, maximizing the camera cooling system's effectiveness and preventing stray IR radiation from entering the camera lens. It was necessary to position each camera at an angle of about 15° off the perpendicular of the surface of the sapphire window. This eliminated any unwanted reflections from the camera lens to the window surface and back to the camera lens.

Operation of the system was labor intensive due to the complexity of infrared theory which dictated constant on-line interaction with the controls, and due to the nature of the tests which included large temperature changes and fast engine transients. For a steady state condition, very little interaction by the operator was necessary assuming the correct sensitivity was chosen to allow the entire field of view's temperature range to be captured in the display temperature range. However, for engine and nozzle transients, constant monitoring was required to insure that valid data was recorded.

DISCUSSION OF RESULTS

Inlet Ducting System

The inlet ducting system performed as designed. Station 1 air flow measurement accuracy was estimated at ±1 percent, well within the desired range (ref. 5). The thrust metric break was maintained with minimal detrimental effect on thrust measurement. It was necessary to periodically remove, clean, and relubricate the inflatable silicone rubber seal. Unless the seal was regularly serviced, drag on the metric portion of the inlet ducting could be erratic and nonlinear. A dry silicon lubricant was successfully used on the clean mating parts. The use of this type of seal was necessary due to the pressure level within the inlet ducting. If low pressures are expected in a future test, a more flexible boot type seal, as used previously in reference 2, would be more appropriate.

Engine and Nozzle Installation

No unexpected problems were encountered due to the engine and nozzle installation. The unreinforced engine fan duct cases limited test operations as described previously. This problem will be corrected as engines are specifically designed for 2D nozzle applications. The manner in which test chamber services for the engine and nozzle crossed the thrust metric break minimized installation drag forces.

Multi-Axis Thrust Measurement System

The axial and lateral thrust measurement system was previously used in another project and had a history of quality measurements. The vertical thrust measurement system was new and it proved to be adequate for this project. Estimated accuracy, as a percent of full scale, for each of the components were as follows: axial ±1 percent; vertical ±5 percent; and lateral ±1 percent. A major problem with the vertical measurement system was the lack of an inline calibration system for each of the three load cells in the system. Although the aft mounted vertical calibration system was adequate for this project, it could not provide high quality calibrations and would not be appropriate for more demanding future projects.

Exhaust Collection System for Vectored Operation

The exhaust collector system performed as designed during all vectored test operations. It was able to withstand the high thermal and pressure loads with no significant deterioration. A factor which helped alleviate the vectored exhaust gas impingement problem was the fact that at the highest heat load conditions (maximum afterburning and maximum nozzle area) mechanical limitations in the nozzle limited the vector angle to about 5°. Recirculation of hot engine exhaust gases back into the test chamber was not significant throughout the entire operating range (between 0° and 20° downward vector angles). The relatively large test chamber cooling air flow was also a factor in minimizing the recirculation. In a future steady state 2D nozzle test where less chamber cooling air and even less recirculation would be desired, remotely operated sliding doors could be installed on the forward end of the collection system. Similar sliding doors were utilized in 1981 during the J-85 2D/CD Versatile Nozzle Project in PSL-3 (ref. 6) to optimize the collector entrance area and position. This concept has limited application for transient testing as the doors can not operate as quickly as the nozzle. Another area of improvement would be the utilization of larger exhaust collector spools. Spools with a diameter of about 2.9 m (9.5 ft) would provide an enhanced collection capability for future projects requiring nozzles vectoring both upward and downward.

Exhaust Collection System for Reverse Operation

A thorough analysis of the reverser exhaust gas collection system operation and its effect on the research engine's performance was completed and reported in reference 4. A summary of the paper's conclusions and recommendations is presented below.

The feasibility of testing a full-scale 2D-CD thrust reversing nozzle in an altitude chamber was successfully demonstrated. The exhaust gas collection system performed adequately over a wide range of operating conditions. Some reverse exhaust gas spillage into the test chamber occurred above 60 percent reverser opening. However, the spillage only created localized chamber heating problems and did not affect engine performance. In fact, engine performance remained unaffected by the collection system over the entire range of thrust reversing operation. A number of reverser collector ducts' internal strengthening rods failed during the testing, but had no effect on the structure due to the low internal operating pressure. One recommendation was to

remove all the internal rods and support the ducts externally with ribs. Additional recommendations included the following: provide longer turning vanes inside each duct to more effectively turn the flow and create a more equally distributed flow field; include some type of seal at the reverser port/collection system interface to minimize exhaust gas spillage (without compromising thrust measurements); and provide a more complete set of instrumentation inside the reverser collector ducts to better define the actual flow field in the ducts.

Instrumentation

The conventional turbine engine instrumentation selected for this project worked very well. Because of the uniqueness of the infrared system application, this section concentrates on its performance and recommendations for system improvements.

Considering the harsh operating environment, the IR systems performed remarkably well. Figure 27 shows a typical IR image. For orientation purposes, the visible image of the nozzle is also presented. This figure shows various shades of grey representing the temperature at points on the nozzle internal surface (note the actual pictures were in color). The accuracy of the IR systems was estimated to be about +3 and -1.5 percent of reading based on pretest blackbody calibration checks. However, accuracy will be affected by changes in emissivity of the object being observed, setting the correct emissivity in the IR controls, the surrounding environment and optical path, and changes in the target angle. An interpretational problem involving accurate resolution (sufficient sensitivity) at higher temperatures was primarily caused by the large temperature range experienced during testing (ambient to about 1450 K (2150 °F)). This problem was accounted for by using a "frame stacking method," i.e., with a very high sensitivity setting, the field of view was recorded with three different temperature ranges such that the high end of one overlaps the low end of the next. In addition, lower temperature data could not be accurately detected and measured because the system was calibrated down to only 477 K (400 °F).

An infrared image can be confusing if the object or field of view is not readily identifiable, especially if the image is a color enhanced one. To avoid this, a 35 mm camera equipped with a 30° by 60° wide angle lens was used to take pictures of the fields of view at each port prior to the installation of each infrared system. These pictures were kept nearby the system operator and provided an accurate visual description of the infrared image on the displays, thus allowing fast and easy correlation between the infrared and visible spectrums.

Although the systems have the capability to enter alpha numeric messages to appear on the displays, the method was cumbersome and time consuming. Therefore, for post run investigations, in order to correlate the images with the test plans, it was necessary to refer back to the project engineer's test log of events. The clock in each IR display was synchronized with the facility clock, so correlation was based on time of day.

Several problems occurred during IR systems operation. Two of the sapphire windows cracked during testing. There appears to be a relationship between the cracking and high temperature operation. The most probable cause

was uneven thermal growth of the large window and its housing. Changes were made to the window housing including more compliant window gaskets, increased cooling air on the hot side of the window, and finally a smaller 5.1 cm (2 in.) diameter window was adapted to the housing. The smaller window adaptation is shown in figure 28. The smaller window, incorporating all the recommended improvements, survived the remaining testing. Several times the camera enclosures exceeded the allowable temperature limit of the Probeye equipment with subsequent loss of picture. Larger expansion coolers were installed in each enclosure and the air was redirected within the enclosures to provide cooling air to most vital areas. In one case, a plastic camera lens housing melted due to radiation from the hot engine exhaust. To eliminate this problem, an aluminum radiation shield was installed around the lens housing and additional cooling air was directed into the area. Argon contamination by dust and moisture also created operational problems for the IR systems. The proper cleaning of system components, and careful use of filters and desiccant dryers eliminated these problems.

CONCLUDING REMARKS

The simulated altitude testing of a 2D-CD vectoring and reversing exhaust nozzle on an advanced F100 derivative engine was successfully accomplished at the NASA Lewis Propulsion Systems Laboratory test chamber 3. All project research objectives were accomplished and the feasibility of testing a full-scale 2D-CD vectoring and thrust reversing nozzle in an altitude chamber was successfully demonstrated.

The inlet ducting system, engine and nozzle installation, and multi-axial thrust measurement system all performed as required. Recommended improvements in these areas included the following: the thrust metric break would have less effect on axial thrust measurement if the inflatable seal was replaced with a more flexible boot-type seal; and the accuracy of the vertical thrust measurement system can be substantially improved if inline calibration systems are provided for each vertical measurement load cell.

The exhaust collection systems for vectored operation and for thrust reversing operation both performed adequately. During vectored operation, the collection system withstood the thermal and pressure loads applied, and captured the vectored engine gases with no significant recirculation of hot gases back into the test chamber. Improvements recommended included incorporating sliding doors on the forward end of the collection system to further minimize recirculation during steady-state tests, and using larger diameter collector spools to improve capture ability for tests requiring vectoring both upward and downward. During reverser operation, the gases were successfully captured and turned downstream. However, a small amount of exhaust gas spillage occurred when the reverser was opened more than 60 percent. The spillage did not affect engine or nozzle performance. To minimize spillage in the future, the use of a flexible seal at the reverser port/collection system interface was suggested along with the incorporation of longer turning vanes inside each reverser duct to more effectively turn the flow and create a more equally distributed flow field.

Considering the harsh operating environment, the IR systems measuring nozzle internal surface temperatures performed remarkably well. All required data were obtained. Data were recorded on VHS tape and on digital disk. The

most significant problem involved cracking the large sapphire windows during high heat load conditions. Adaptation of a smaller, better cooled window solved the problem.

REFERENCES

1. Biesiadny, T.; Burkhardt, L.; and Braithwaite, W.: Uniform Engine Testing Program, Phase I. NASA TM-82978, 1982.

2. Blozy, J.T.: Altitude Testing of the 2D V/STOL ADEN Demonstrator on an F404 Engine. NASA CR-174824, 1984.

3. Three Component Thrust Stand. NASA Contract NAS3-23115, Ormond, Inc., Santa Fe Springs, CA, 1981.

4. Mehalic, C.M.; and Lottig, R.A.: Full-Scale Thrust Reverser Testing in an Altitude Facility. AIAA Paper 87-1788, June 1987. (Also NASA TM-88967.)

5. Abdelwahab, M.; and Biesiadny, T.J.: Measurement Uncertainty for the Uniform Engine Testing Program Conducted at NASA Lewis Research Center. NASA TM-88943, 1987.

6. Straight, D.M.; and Cullom, R.R.: Thrust Performance of a Variable-Geometry, Nonaxisymmetric, Two-Dimensional, Convergent-Divergent Exhaust Nozzle on a Turbojet Engine at Altitude. NASA TP-2171, 1983.

APPENDIX A

CALCULATION OF INLET TOTAL AIRFLOW

The method used in the altitude test facilities at NASA to calculate inlet total airflow at the airflow station, station 1, (see fig. 24 for station locations) involved the integration of a flow per unit area calculated for each total pressure probe. The highlights of this method are presented below.

At station 1, four boundary layer rakes with eight immersions were used to measure the total pressure profile. The immersions, as shown in figure A1, were labeled from r_B at the wall to r_o in the freestream:

Dividing station 1 into rings, one for each probe radius, the integral

$$\int \frac{W}{A}\, dA$$

was evaluated for each ring where

$$\frac{W}{A} = \frac{P_s}{\sqrt{RT}} \sqrt{\frac{2\gamma}{\gamma - 1}\left[\left(\frac{P_t}{P_s}\right)^{(\gamma-1)/\gamma} - 1\right]\left(\frac{P_t}{P_s}\right)^{(\gamma-1)/\gamma}}$$

The nomenclature for the above equation is as follows:

W airflow

A area

P_t average of all probes at r_i

P_s average of all four wall static probes at station 1

T average of thirteen total temperature probes at plenum station

R gas constant for air

γ specific heat

Two assumptions were made for this method of determining airflow. The first is that no heat transfer occurred between the plenum station and station 1. The second assumption was that the static pressure profile across the duct at station 1 was constant. This assumption was checked through surveys made during similar NASA test projects such as reference 1.

APPENDIX B

DETERMINATION OF GROSS THRUST

Calculation of Gross Thrust

Net thrust is defined as the difference between gross thrust and the ram force term $W_{AE} * V_O$. Net thrust has application only in a purely axial thrust mode (for determination of specific fuel consumption). Since this item was of little interest for the 2D/CD project, this discussion will focus on determination of multi-axis gross thrust.

Axial gross thrust. - For this axis, the summation of forces acting on the engine is equal to the difference between the engine exhaust mommentum ($W_E V_E$) and the engine inlet momentum ($W_{AI} V_I$), using the conservation of momentum principle. Since the test is performed in an altitude test facility, pressure-area forces and test installation calibration tare forces are a factor in gross thrust determination.

Referencing figure B1(a), with pressures referenced to cell pressure, P_{AMB}, the momentum equation summation is as follows:

$$F_{MA} + A_I(P_{SI} - P_{AMB}) - A_E(P_{SE} - P_{AMB}) + \int_{A_I}^{A_E} (P - P_{AMB})dA$$

$$- A_S(P_{SS} - P_{AMB}) - F_{DRAG} = W_E V_E - W_{AI} V_I$$

Engine axial gross thrust is defined as follows:

$$F_{GA} = W_E V_E = A_E(P_{SE} - P_{AMB})$$

Rearranging terms, the following equation is used to define axial gross thrust:

$$F_{GA} = F_{MA} + W_{AI} V_I + A_I(P_{SI} - P_{AMB}) - A_S(P_{SS} - P_{AMB}) - F_{DRAG} + \int_{A_I}^{A_E} (P - P_{AMB})dA \qquad (1)$$

The nomenclature for equation (1) is as follows:

F_{GA}	gross axial thrust
F_{MA}	measured axial thrust
$W_{AI} V_I$	momentum of air flow at engine inlet (metric break)
$A_I(P_{SI} - P_{AMB})$	force at engine inlet resulting from difference between inlet duct static pressure and test cell static pressure

$A_S(P_{SS} - P_{AMB})$ force at inlet seal using equivalent seal area (A_S) as multiplied by the difference between seal static pressure and test cell static pressure

F_{DRAG} calibrated drag load resulting from test cell cooling air impingement on engine, mount hardware, and duct work

$\int_{A_I}^{A_E} (P - P_{AMB})dA$ forces on cowl surfaces resulting from differences between cowl surface static pressure and test cell ambient static pressure

Vertical gross thrust. - The summation of forces in the vertical direction acting on the engine is equal to the vertical component of vectored engine exhaust momentum ($W_E V_E$) only, since inlet momentum is totally axial. Drag forces and seal forces are not a factor, since they are axial. However, a vertical force associated with inlet deflection has to be taken in account, as are differential cowl pressure forces in the vertical direction.

Referencing figure B1(b), with pressures referenced to cell pressure, P_{AMB}, the momentum equation summation is as follows:

$$A_{EV}(P_{SE} - P_{AMB}) + \int_{A_L}^{A_U} (P - P_{AMB})dA + F_{MVF} + F_{MVS} - F_{MVR} = -\left[W_E V_E\right]_V$$

Engine vertical gross thrust is defined as follows:

$$F_{GV} = \left[W_E V_E\right]_V + A_{EV}(P_{SE} - P_{AMB})$$

Rearranging terms, the following equation is used to define vertical gross thrust:

$$F_{GV} = F_{MVR} - F_{MVF} - F_{MVS} - \int_{A_L}^{A_U} (P - P_{AMB})dA \qquad (2)$$

The nomenclature for equation (2) is as follows:

F_{GV} gross vertical thrust

F_{MVR} measured vertical thrust, aft load cell locations

F_{MVF} measured vertical thrust, forward load cell location

F_{MVS} measured vertical thrust resulting from inlet deflection

$\int_{A_L}^{A_U} (P - P_{AMB})dA$ pressure loads on augmentor surfaces (vertical components) resulting from differences between augmentor surface static pressures and test cell ambient static pressure

Lateral gross thrust. - For the lateral axis, no inlet or exhaust momentum terms are involved. However, side loads resulting from pressurized process system lines or other miscellaneous sources are taken into account and measured with the forward and aft lateral load cells. The lateral gross thrust equation is then simply the difference between the two load cell readings.

$$F_{GH} = F_{MHR} - F_{MHF} \tag{3}$$

F_{GH} (lateral gross thrust), F_{MHR} (lateral force, aft location), and F_{MHF} (lateral force, forward location) is the nomenclature for the above equation.

Resultant gross thrust. - The resultant gross thrust, F_{GR}, is the square root of the sum of the squares of equations (1) to (3) above:

$$F_{GR} = \sqrt{(F_{GA})^2 + (F_{GV})^2 + (F_{GH})^2} \tag{4}$$

Determination of Multi-Axis Thrust Stand Load Cell Interaction Coefficients

It is assumed that no second order interactions are present between the four in-frame thrust measuring systems, and that all calibrations are linear and can be represented by a straight line through the data. The thrust measurement load cell readings can be defined by the following:

$$\text{Axial; } F_{DA} = F_{CA}\left(\frac{\partial F_{DA}}{\partial F_{CA}}\right) + F_{CHF}\left(\frac{\partial F_{DA}}{\partial F_{CHF}}\right) + F_{CHR}\left(\frac{\partial F_{DA}}{\partial F_{CHR}}\right) + F_{CV}\left(\frac{\partial F_{DA}}{\partial F_{CV}}\right) \tag{5}$$

$$\text{Forward lateral; } F_{DHF} = F_{CA}\left(\frac{\partial F_{DHF}}{\partial F_{CA}}\right) + F_{CHF}\left(\frac{\partial F_{DHF}}{\partial F_{CHF}}\right) + F_{CHR}\left(\frac{\partial F_{DHF}}{\partial F_{CHR}}\right) + F_{CV}\left(\frac{\partial F_{DHF}}{\partial F_{CV}}\right) \tag{6}$$

$$\text{Aft lateral; } F_{DHR} = F_{CA}\left(\frac{\partial F_{DHR}}{\partial F_{CA}}\right) + F_{CHF}\left(\frac{\partial F_{DHR}}{\partial F_{CHF}}\right) + F_{CHR}\left(\frac{\partial F_{DHR}}{\partial F_{CHR}}\right) + F_{CV}\left(\frac{\partial F_{DHR}}{\partial F_{CV}}\right) \tag{7}$$

$$\text{Vertical; } F_{DV} = F_{CA}\left(\frac{\partial F_{DV}}{\partial F_{CA}}\right) + F_{CHF}\left(\frac{\partial F_{DV}}{\partial F_{CHF}}\right) + F_{CHR}\left(\frac{\partial F_{DV}}{\partial F_{CHR}}\right) + F_{CV}\left(\frac{\partial F_{DV}}{\partial F_{CV}}\right) \tag{8}$$

The force nomenclature is as follows:

F_{DA} measured axial thrust

F_{CA} calibration (applied) axial load

F_{DHF} indicated forward lateral thrust

F_{CHF} calibration (applied) forward lateral load

F_{DHR} indicated aft lateral thrust

F_{CHR} calibration (applied) aft lateral load

F_{DV} indicated vertical thrust

F_{CV} calibration (applied) vertical load

The partial differentials in the above equations can be denoted by coefficients, K_1, through K_{16}. Thus, equations (5) to (8) can be expressed as follows:

$$F_{DA} = K_1F_{CA} + K_2F_{CHF} + K_3F_{CHR} + K_4F_{CV}$$

$$F_{DHF} = K_5F_{CA} + K_6F_{CHF} + K_7F_{CHR} + K_8F_{CV}$$

$$F_{DHR} = K_9F_{CA} + K_{10}F_{CHF} + K_{11}F_{CHR} + K_{12}F_{CV}$$

$$F_{DV} = K_{13}F_{CA} + K_{14}F_{CHF} + K_{15}F_{CHR} + K_{16}F_{CV}$$

The coefficients, K_1 to K_{16}, are determined as follows: a range of known loads are applied at each calibration location. For each applied load, the indicated load cell readings in all axes are recorded. This information is shown graphically in figure B2 for the axial applied load, F_{CA}. Graphs for F_{CHF}, F_{CHR}, and F_{CV} are similar to F_{CA}, shown in figure B2.

Equations (5) to (8) can be expressed in matrix notation:

$$\begin{Bmatrix} F_{DA} \\ F_{DHF} \\ F_{DHR} \\ F_{DV} \end{Bmatrix} = \begin{bmatrix} K_1 & K_2 & K_3 & K_4 \\ K_5 & K_6 & K_7 & K_8 \\ K_9 & K_{10} & K_{11} & K_{12} \\ K_{13} & K_{14} & K_{15} & K_{16} \end{bmatrix} \begin{Bmatrix} F_{CA} \\ F_{CHF} \\ F_{CHR} \\ F_{CV} \end{Bmatrix} \tag{9}$$

Since equation (9) describes indicated thrust forces in terms of the interaction coefficients multiplied by actual (applied) thrust forces, the matrix has to be inverted, so that actual forces can be determined from indicated values. The equation with the inverted matrix is as follows:

$$\begin{Bmatrix} F_{CA} \\ F_{CHF} \\ F_{CHR} \\ F_{CV} \end{Bmatrix} = \begin{bmatrix} K_1 & K_2 & K_3 & K_4 \\ K_5 & K_6 & K_7 & K_8 \\ K_9 & K_{10} & K_{11} & K_{12} \\ K_{13} & K_{14} & K_{15} & K_{16} \end{bmatrix}^{-1} \begin{Bmatrix} F_{DA} \\ F_{DHF} \\ F_{DHR} \\ F_{DV} \end{Bmatrix} \tag{10}$$

The inverted coefficients in equation (11) result in 16 contants, C_1 to C_{16}. Since the matrix inversion gives actual loads in terms of indicated loads, the C subscript may be removed from the left side of the equation and replaced with subscript M (for measured force). Equation (10) can then be represented in matrix form as follows:

$$\begin{Bmatrix} F_{MA} \\ F_{MHF} \\ F_{MHR} \\ F_{MV} \end{Bmatrix} = \begin{bmatrix} C_1 & C_2 & C_3 & C_4 \\ C_5 & C_6 & C_7 & C_8 \\ C_9 & C_{10} & C_{11} & C_{12} \\ C_{13} & C_{14} & C_{15} & C_{16} \end{bmatrix} \begin{Bmatrix} F_{DA} \\ F_{DHF} \\ F_{DHR} \\ F_{DV} \end{Bmatrix} \tag{11}$$

Expressing the matrix in equation form

$$F_{MA} = C_1 F_{DA} + C_2 F_{DHF} + C_3 F_{DHR} + C_4 F_{DV} \tag{12}$$

$$F_{MHF} = C_5 F_{DA} + C_6 F_{DHF} + C_7 F_{DHR} + C_8 F_{DV} \tag{13}$$

$$F_{MHR} = C_9 F_{DA} + C_{10} F_{DHF} + C_{11} F_{DHR} + C_{12} F_{DV} \tag{14}$$

$$F_{MV} = C_{13} F_{DA} + C_{14} F_{DHF} + C_{15} F_{DHR} + C_{16} F_{DV} \tag{15}$$

where F_{MA}, F_{MHF}, F_{MHR}, and F_{MV} are the measured axial, forward lateral, aft lateral, and vertical forces respectively acting on the multi-axis thrust stand.

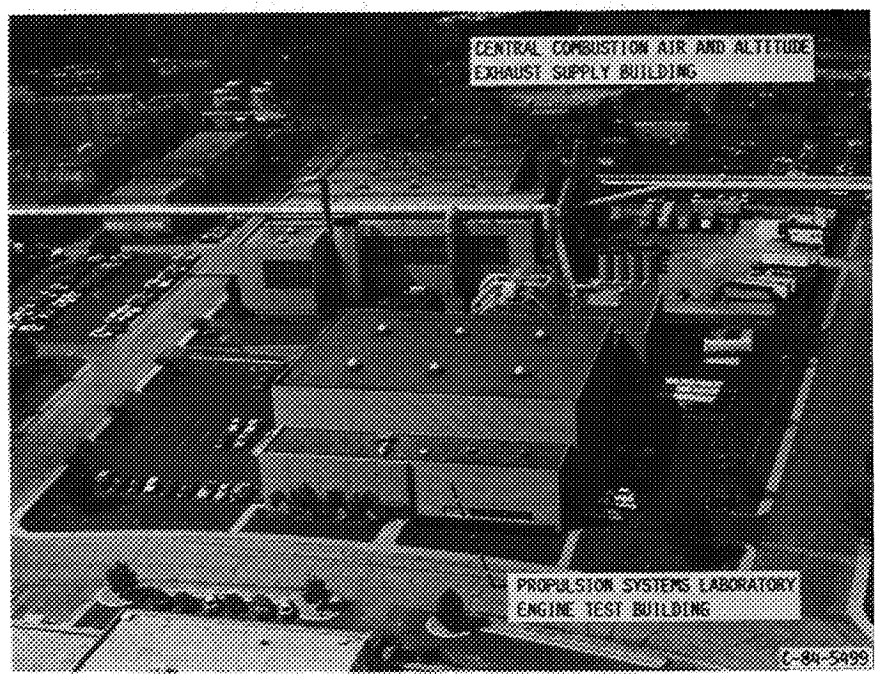

FIGURE 1. - PROPULSION SYSTEMS LABORATORY COMPLEX.

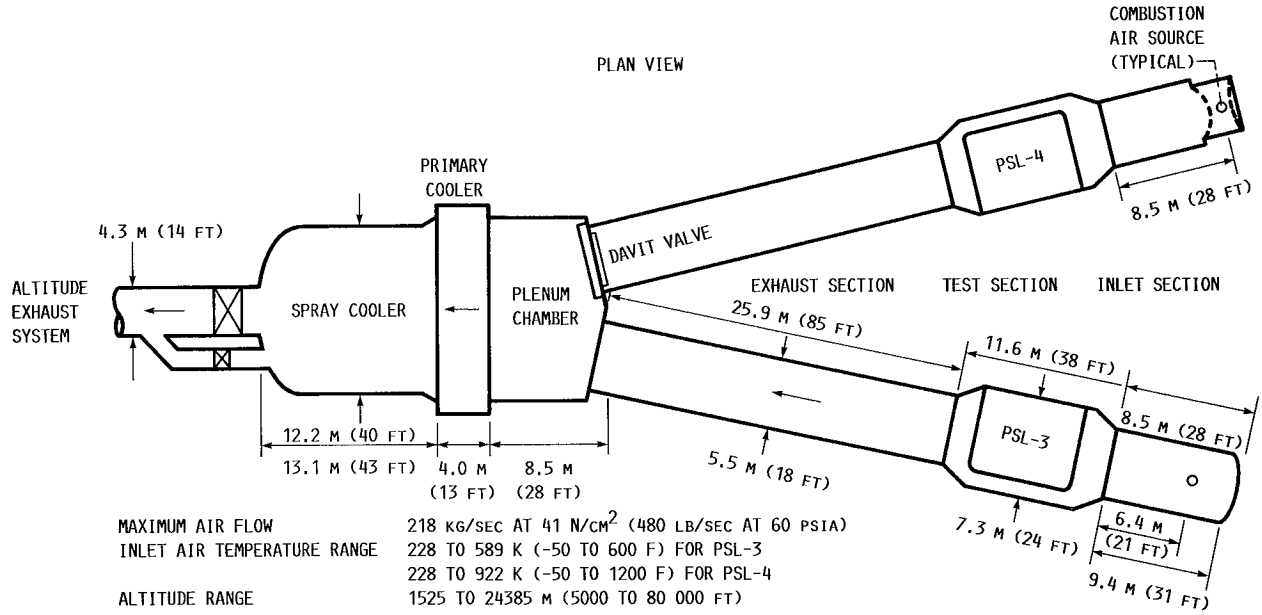

FIGURE 2. - PROPULSION SYSTEMS LABORATORY LAYOUT AND CAPABILITIES.

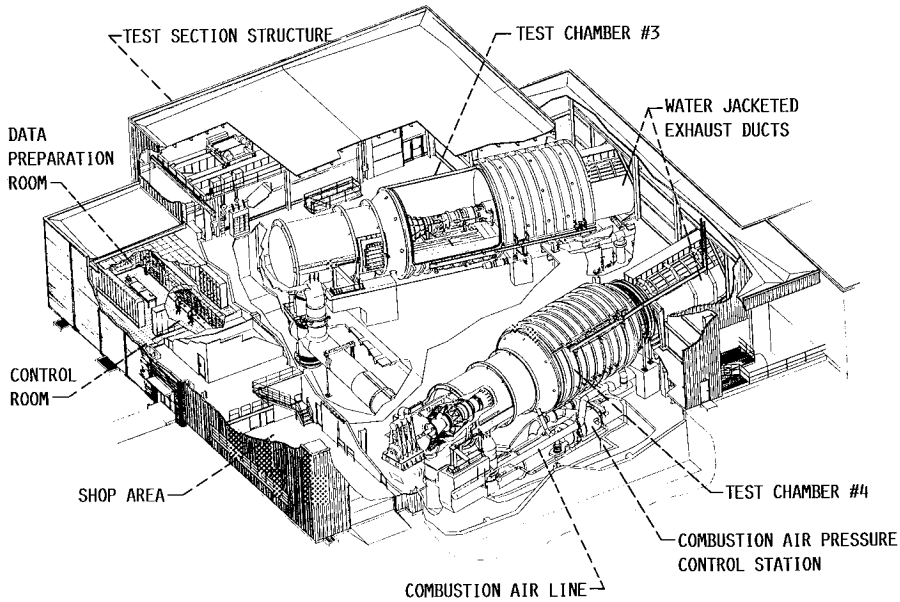

FIGURE 3. - CUTAWAY VIEW OF PROPULSION SYSTEMS LABORATORY.

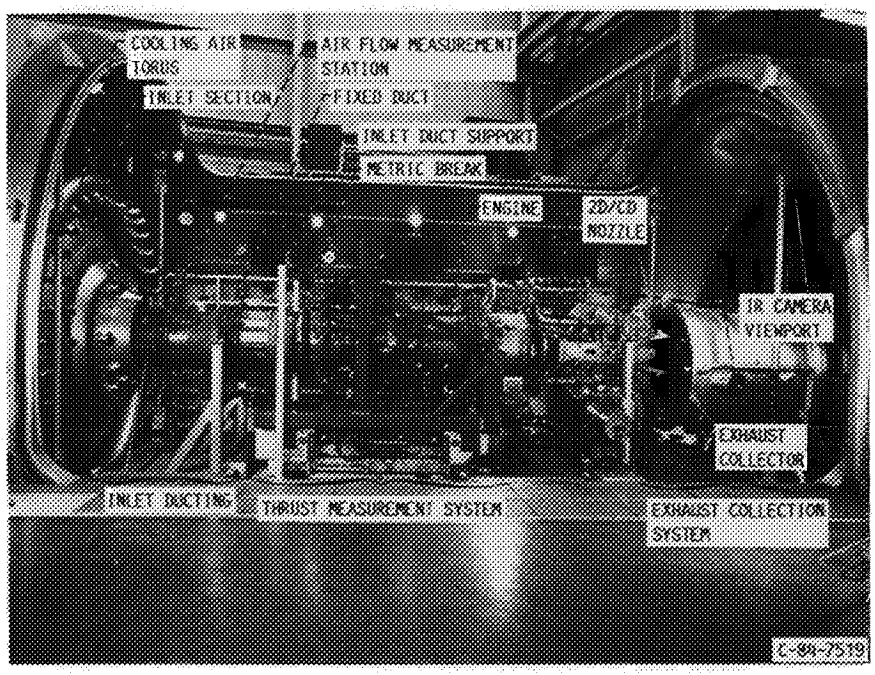

FIGURE 4. - OVERALL INSTRALLATION OF TEST HARDWARE IN TEST CELL #3 (VECTORED CONFIGURATION)

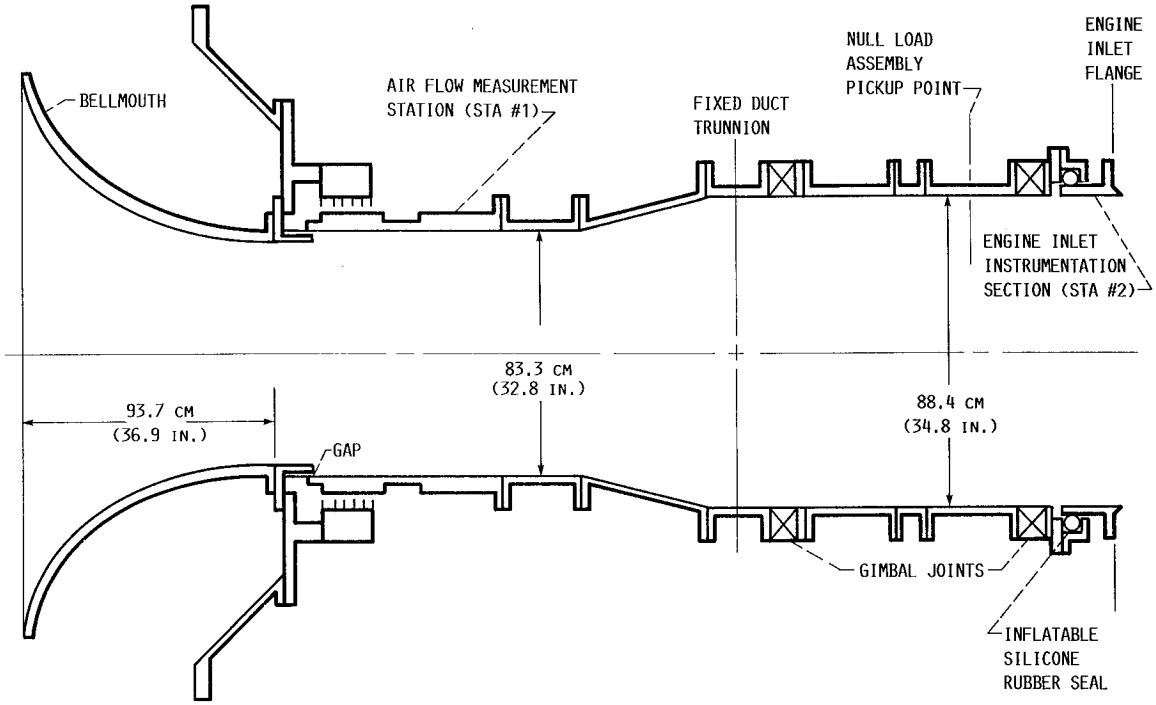

FIGURE 5. - INLET DUCTING ARRANGEMENT.

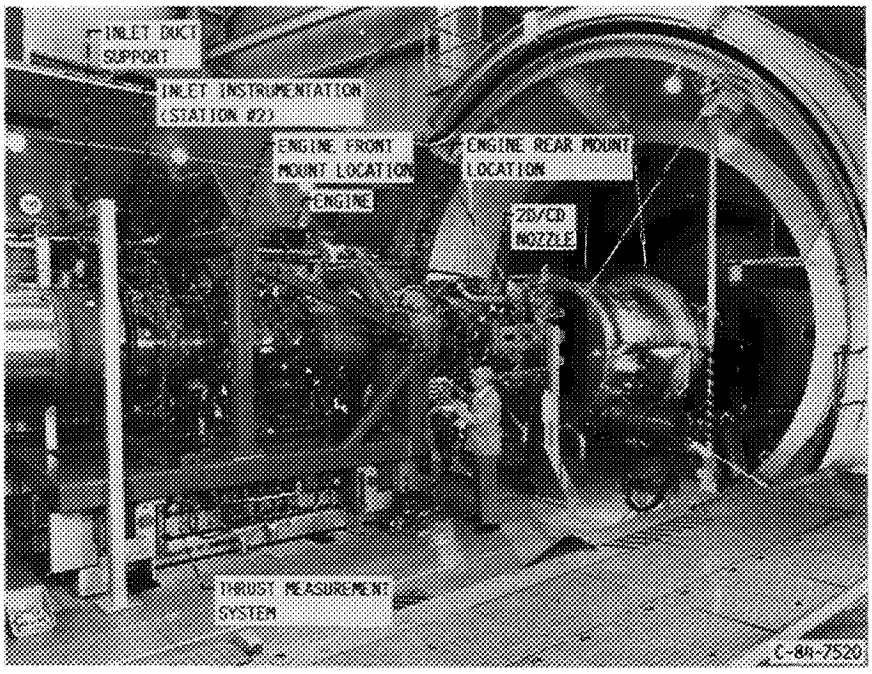

FIGURE 6. - ENGINE AND NOZZLE INSTALLATION.

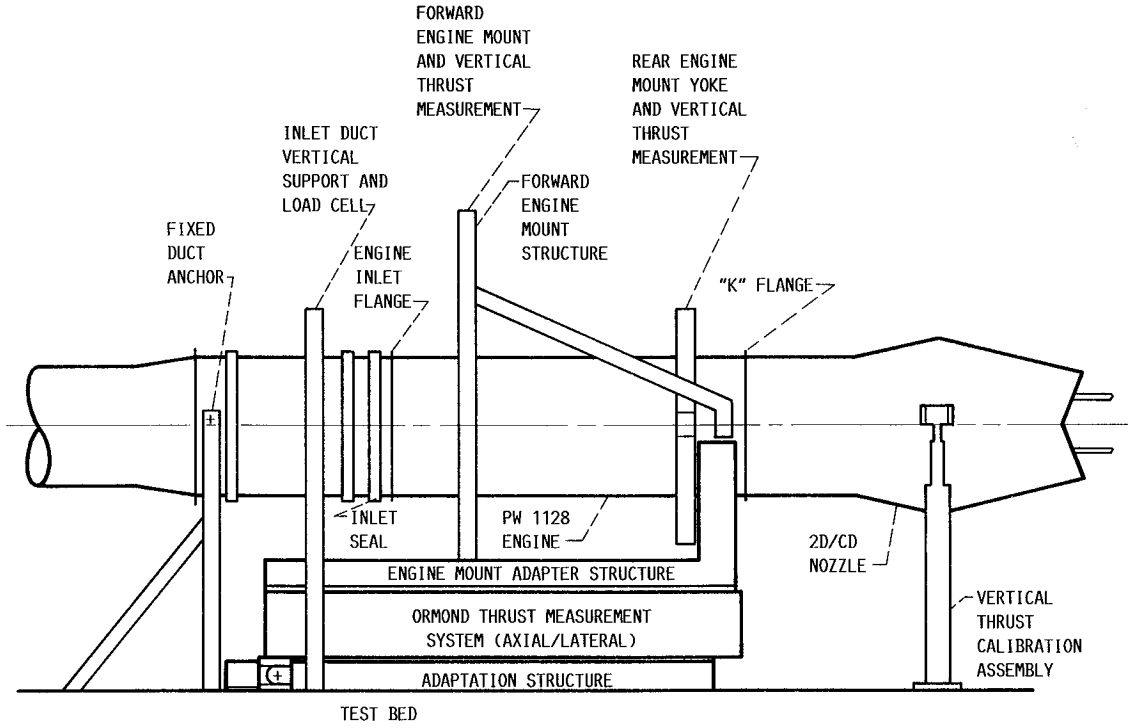

FIGURE 7. - ENGINE MOUNTING SYSTEM.

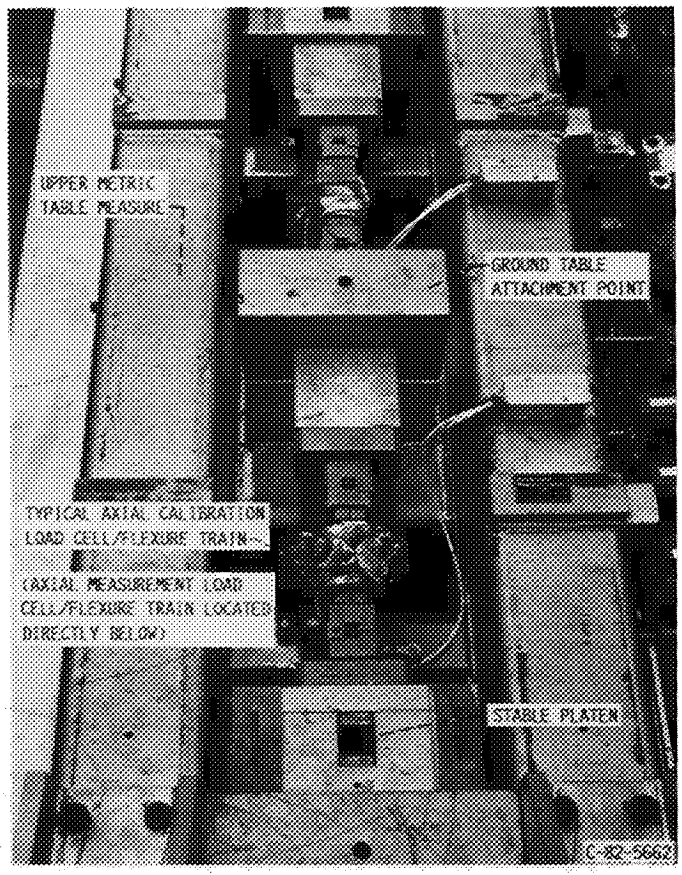

(A) AXIAL SYSTEM (VIEWED FROM ABOVE).

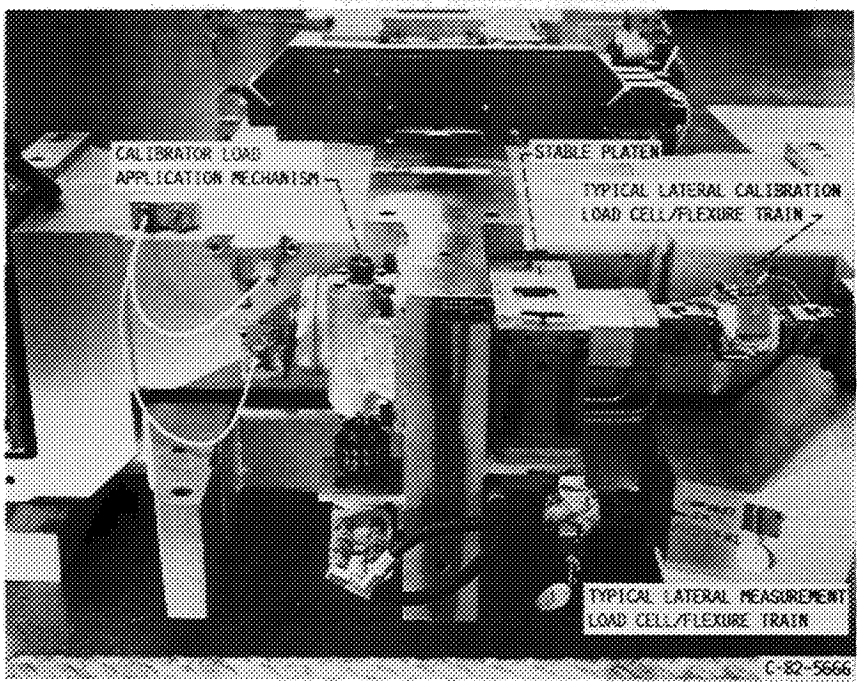

(B) FORWARD LATERAL SYSTEM (VIEWED FROM REAR).

FIGURE 8. - AXIAL AND LATERAL THRUST MEASUREMENT SYSTEMS.

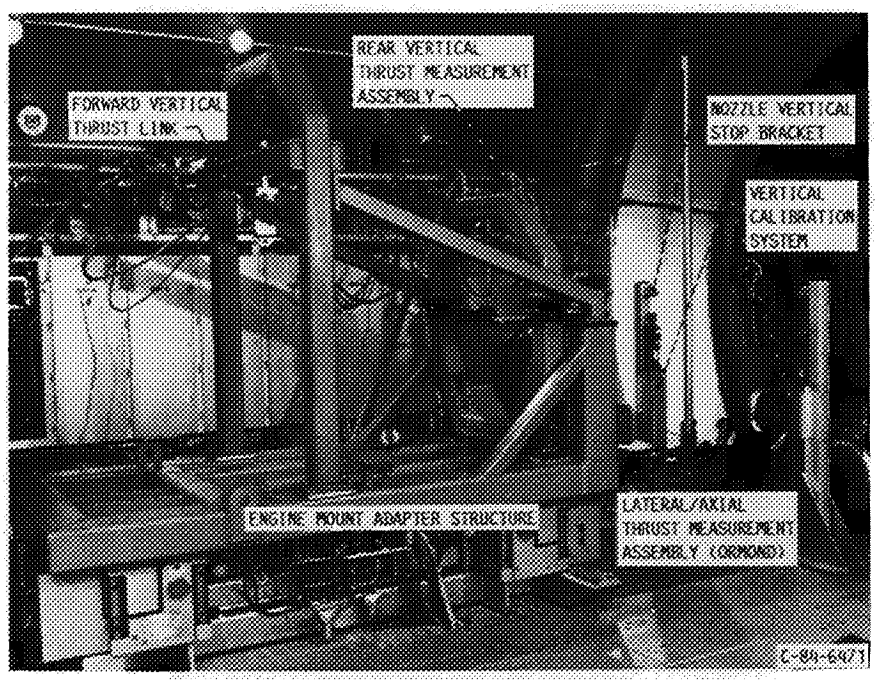

FIGURE 9. - THRUST MEASUREMENT SYSTEM (W/O ENGINE AND NOZZLE).

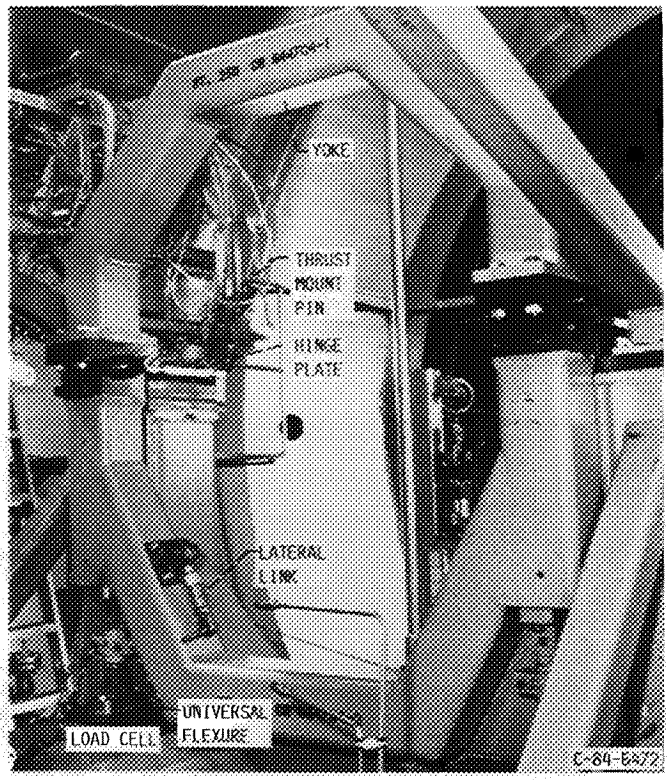

(A) UPSTREAM VIEW.

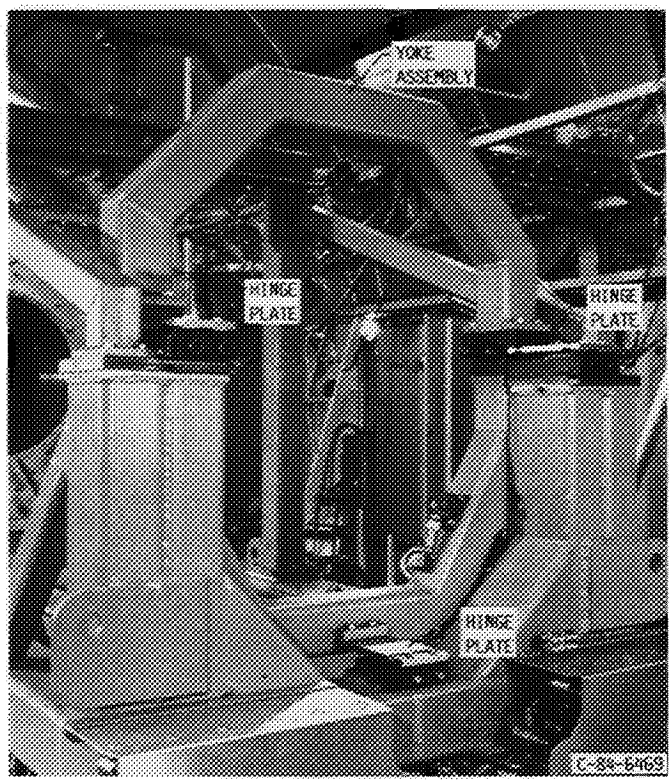

(B) DOWNSTREAM VIEW.

FIGURE 10. - REAR MOUNT VERTICAL THRUST MEASUREMENT SYSTEM.

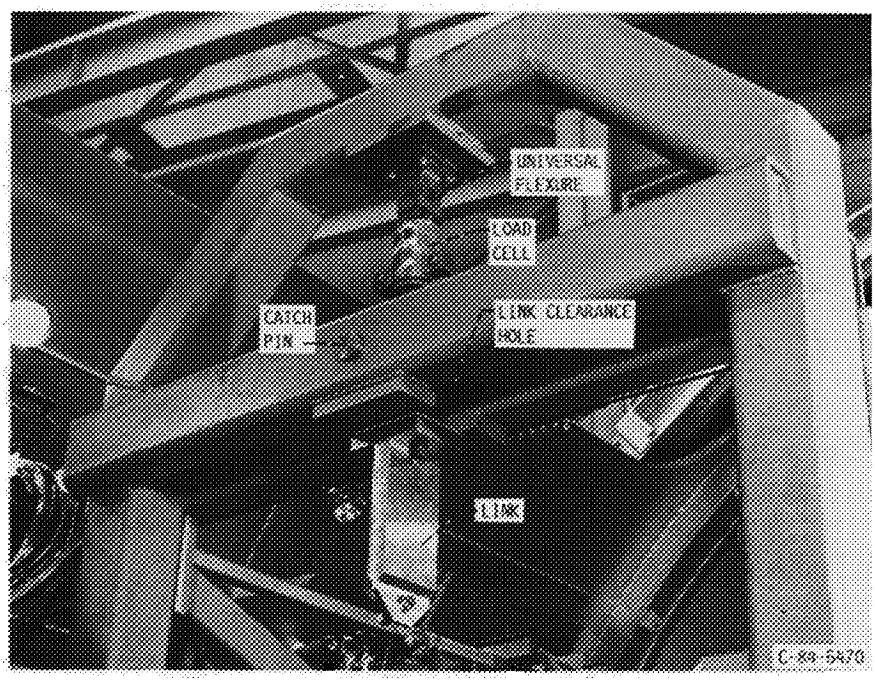

FIGURE 11. - VERTICAL THRUST LINK, VERTICAL THRUST MEASUREMENT SYSTEM (UPSTREAM VIEW).

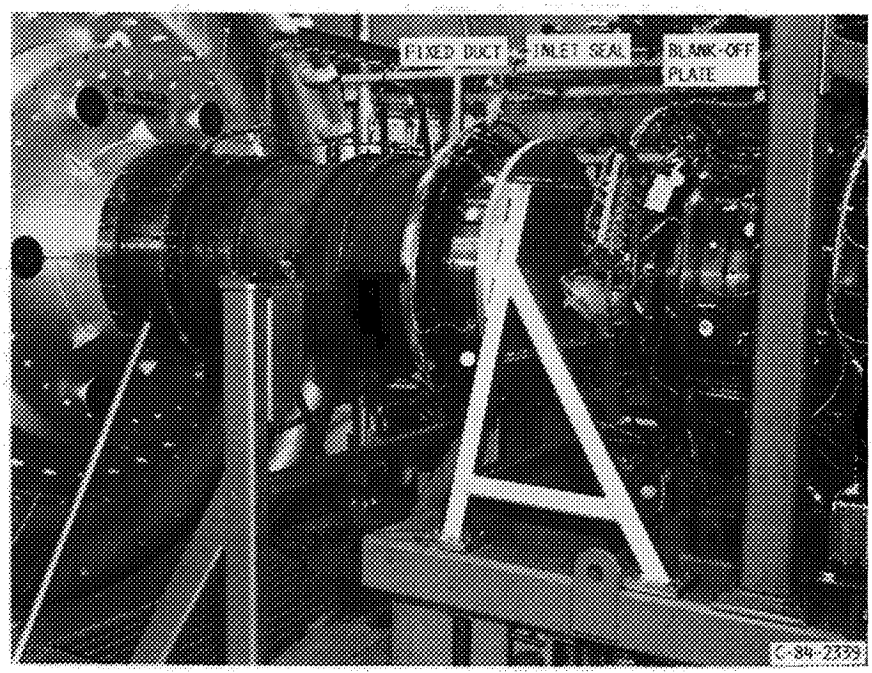

FIGURE 12. - ENGINE INLET SEAL FORCE CALIBRATION CONFIGURATION.

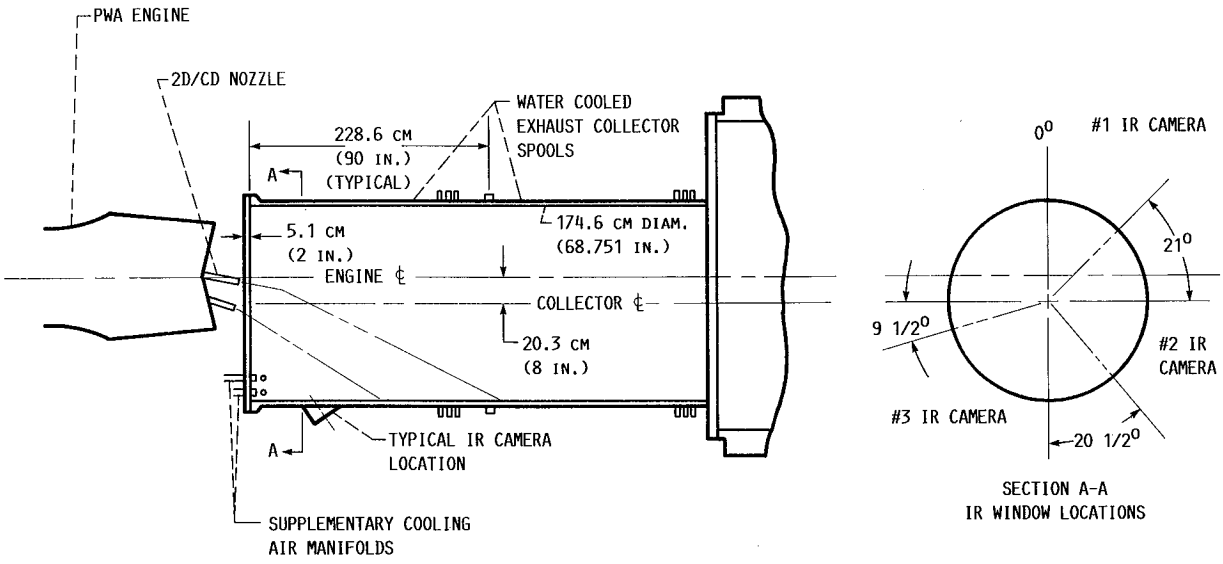

3.8 CM (1 1/2 IN.) PIPE 86.2 N/CM (125 PSIG)

FIGURE 13. - EXHAUST COLLECTOR CONFIGURATION FOR VECTORED OPERATION.

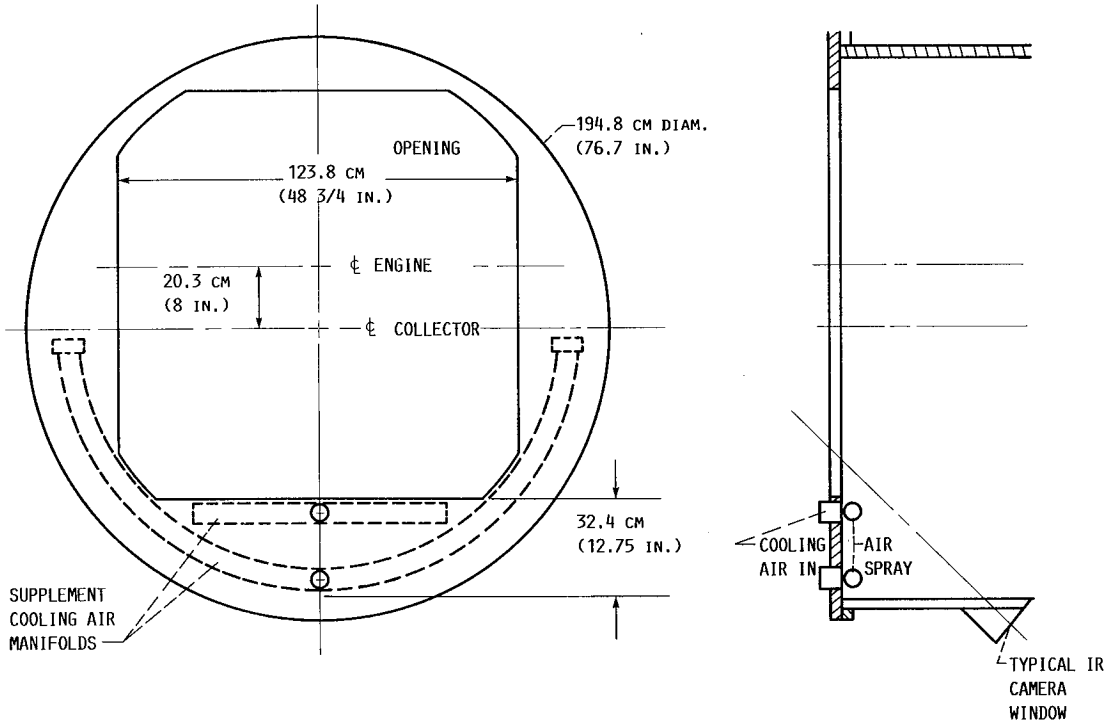

FIGURE 14. - EXHAUST COLLECTOR FRONT ADAPTER PLATE FOR VECTORED OPERATION.

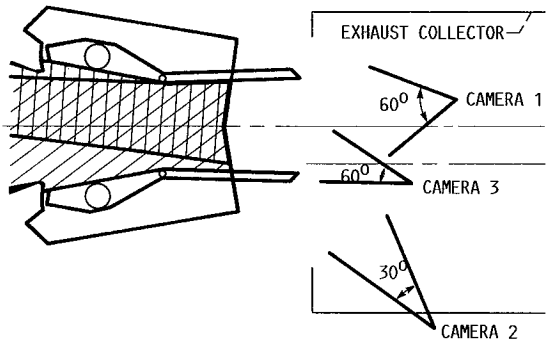

(A) A/B-VECTOR ANGLE 0°.

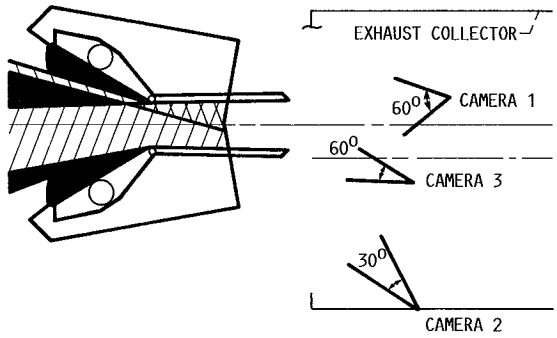

(B) NON A/B-VECTOR ANGLE 0°.

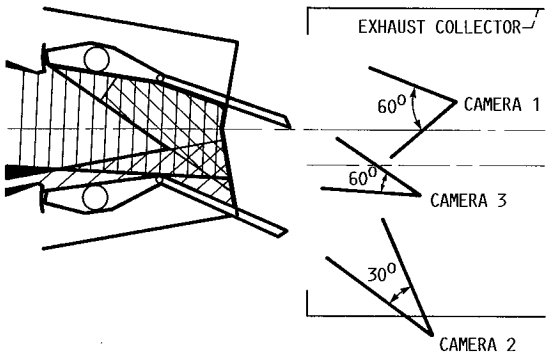

(C) A/B-VECTOR ANGLE 20°.

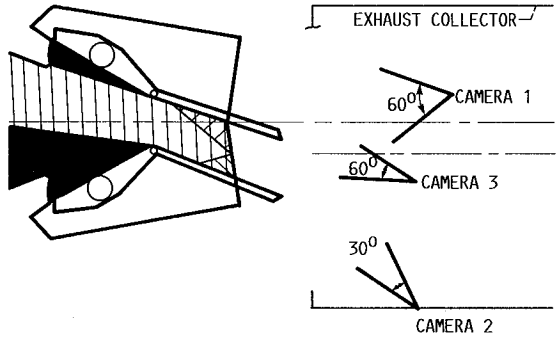

(D) NON A/B-VECTOR ANGLE 20°.

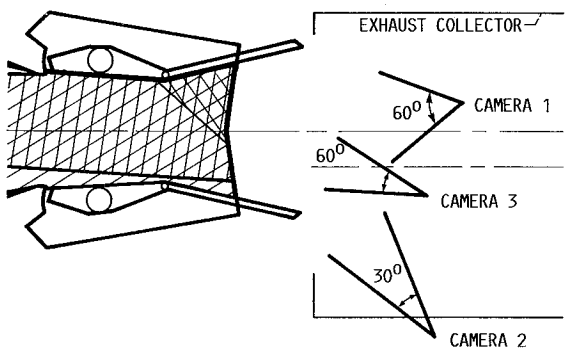

INDICATES AREA NOT VISIBLE TO ANY CAMERA

CROSSHATCHING INDICATES AREAS OF SIDEWALL SEEN BY CAMERAS AT A VIEWING ANGLE > 20°

(E) A/B-MAXQ.

FIGURE 15. - INFRARED CAMERA POSITIONS.

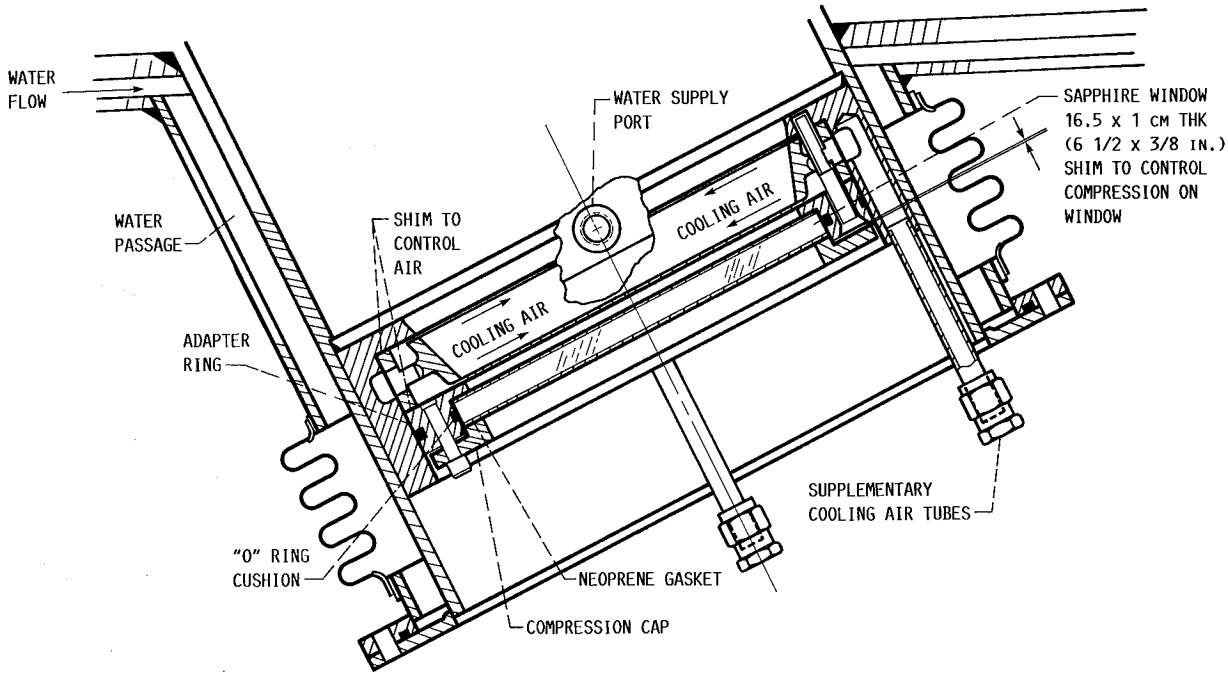

FIGURE 16. - DETAIL OF INFRARED CAMERA WINDOW INSTALLATION (INITIAL CONFIGURATION).

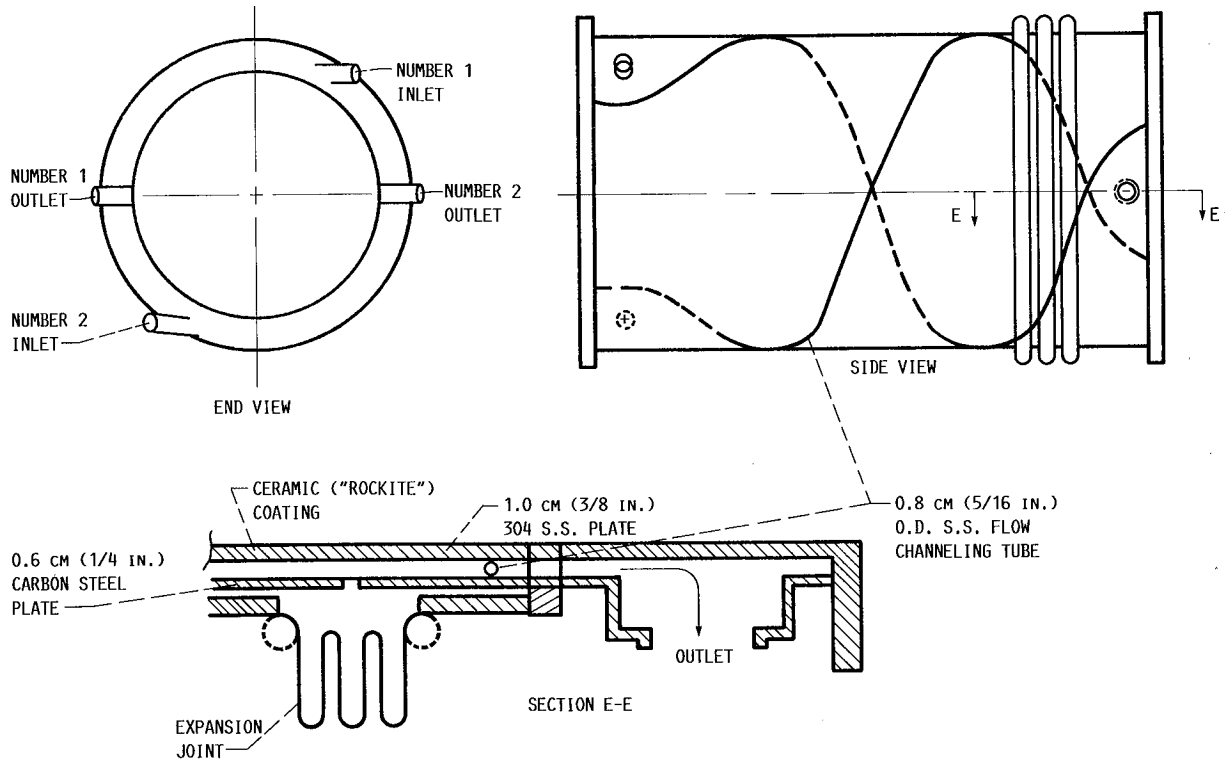

FIGURE 17. - BASIC EXHAUST COLLECTOR WATER COOLED SPOOL.

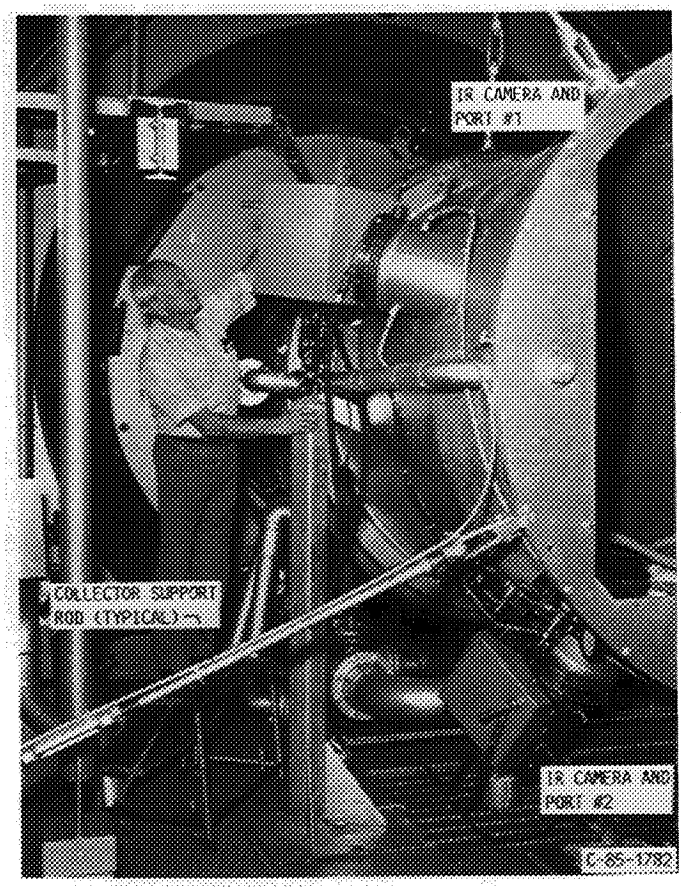

FIGURE 18. - FORWARD COLLECTOR SPOOL INSTALLATION.

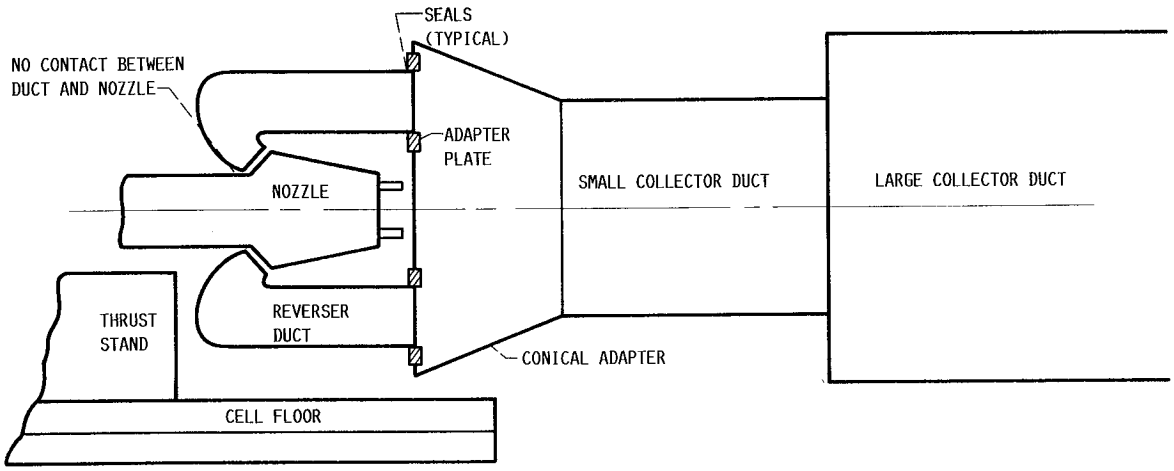

FIGURE 19. - EXHAUST COLLECTOR CONFIGURATION FOR REVERSE OPERATION.

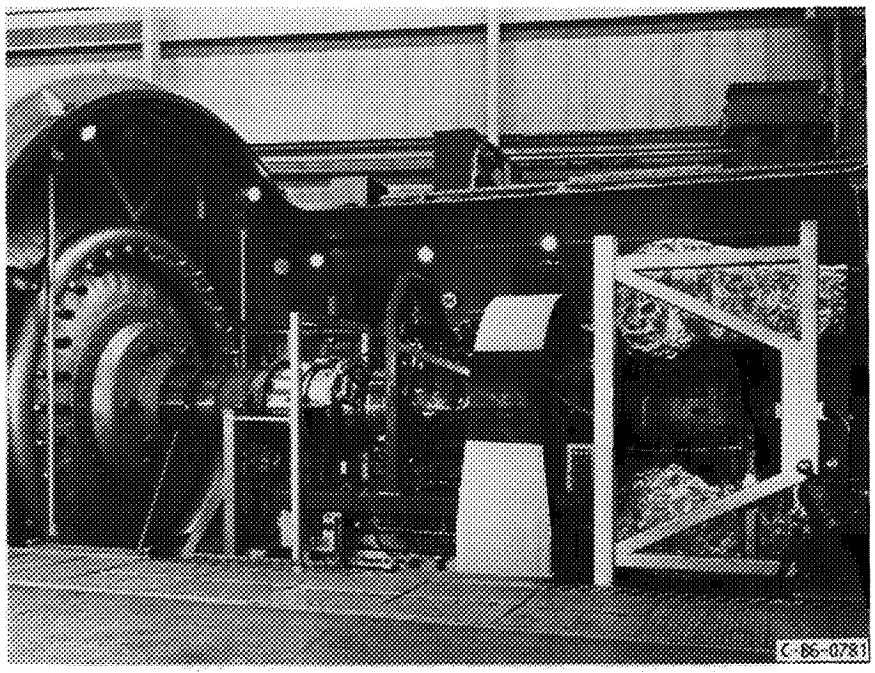

FIGURE 20. - ENGINE AND NOZZLE INSTALLATION FOR REVERSE OPERATION.

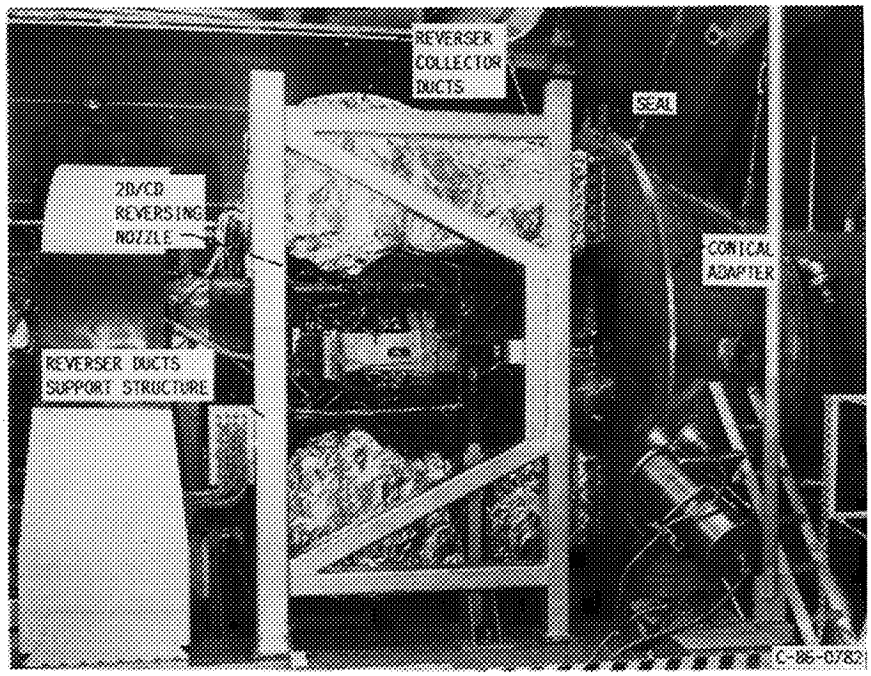

FIGURE 21. - CLOSE-UP VIEW OF NOZZLE, REVERSER COLLECTOR DUCTS AND CONICAL ADAPTER.

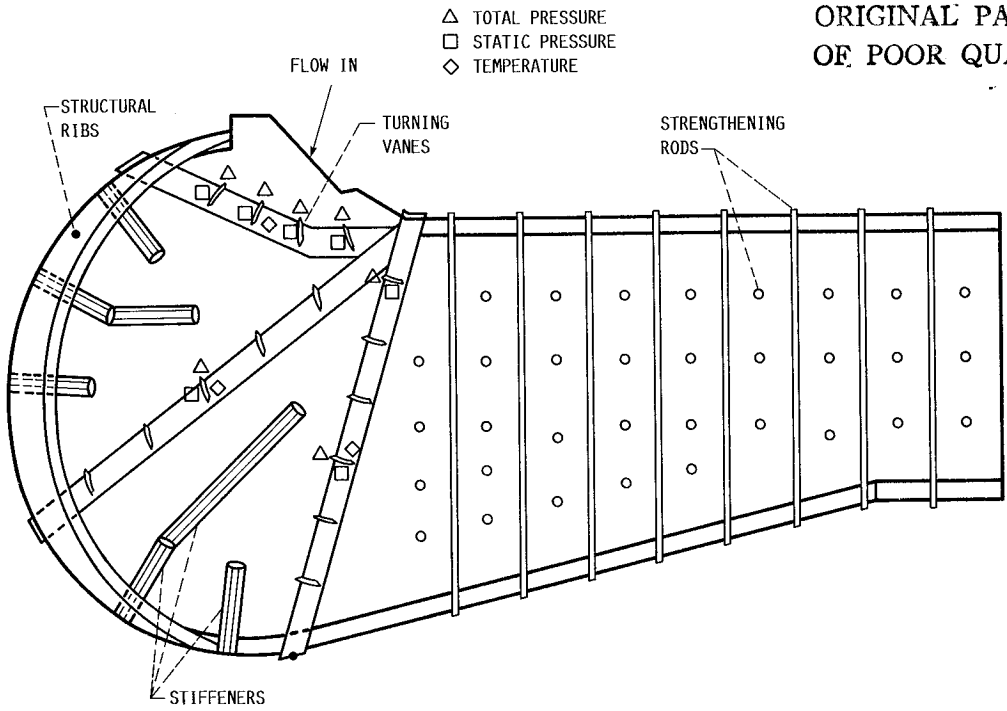

FIGURE 22. - INTERNAL DETAILS OF A REVERSER COLLECTOR DUCT.

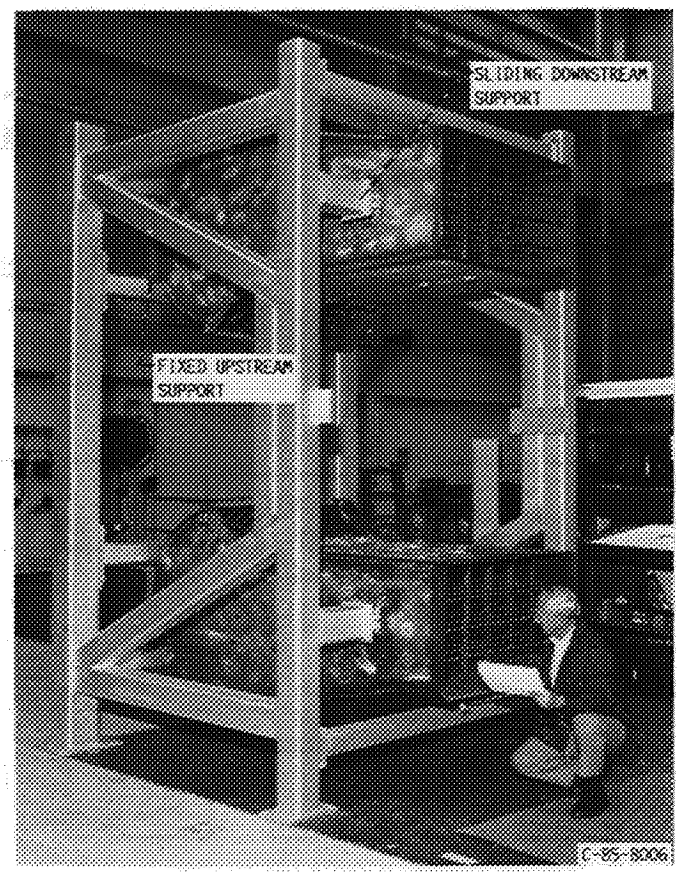

FIGURE 23. - REVERSER COLLECTOR DUCTS MOUNTING SYSTEM.

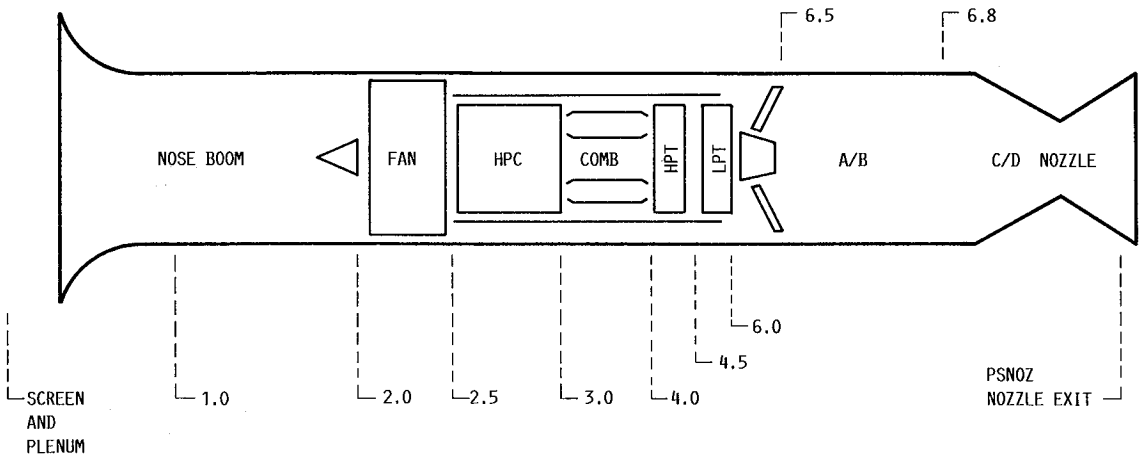

ENGINE STATION LOCATIONS

STATION	LOCATION	STATION	LOCATION	STATION	LOCATION
1.0	AIRFLOW MEASURING STATION	3.0	HPC EXIT	6.0	LPT EXIT
2.0	FAN INLET	4.0	COMBUSTOR EXIT/ HPT INLET	6.5	AUGMENTOR INLET
2.5	FAN EXIT/ HPC INLET	4.5	HPT EXIT/LPT INLET	6.8	NOZZLE INLET

FIGURE 24. - SUMMARY OF ENGINE RELATED INSTRUMENTATION.

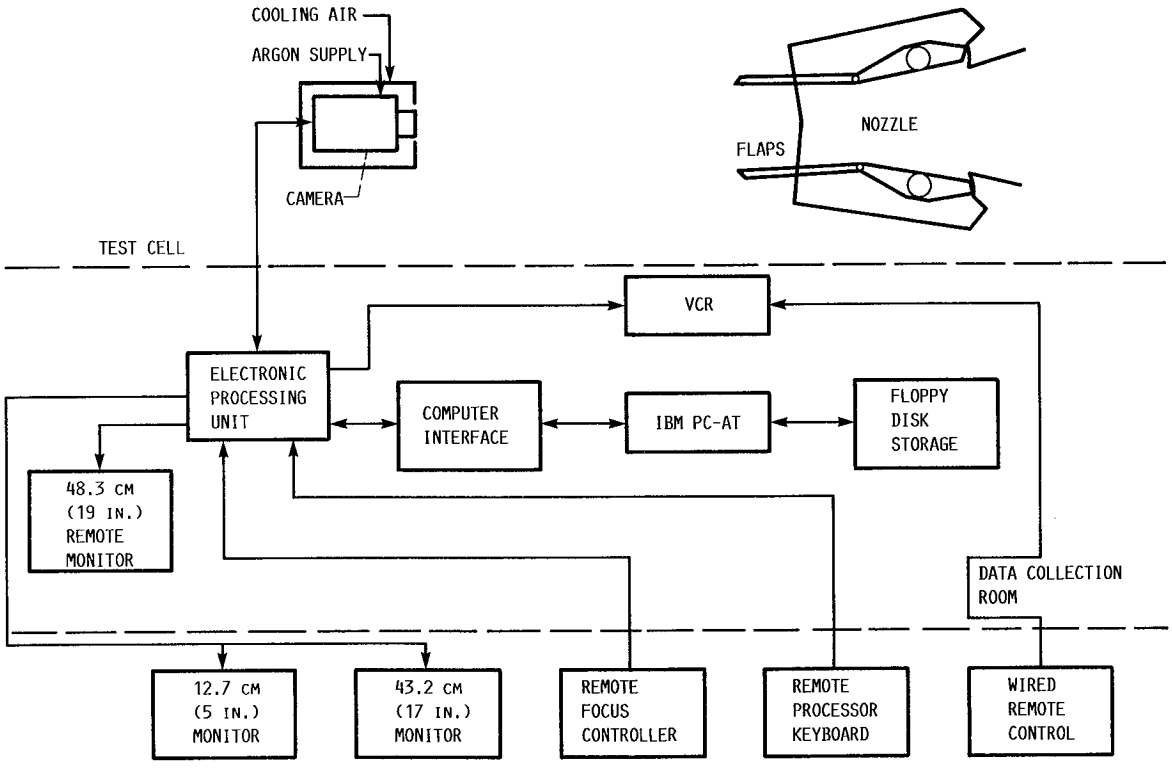

FIGURE 25. - TYPICAL IR SYSTEM CONFIGURATION.

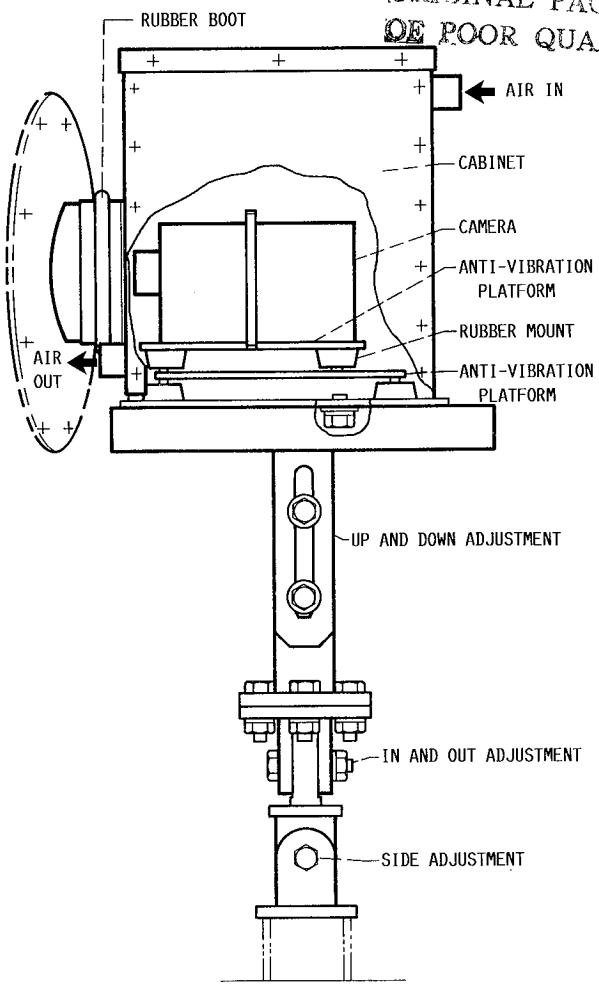

FIGURE 26. - INFRARED CAMERA ENCLOSURE AND MOUNT SYSTEM.

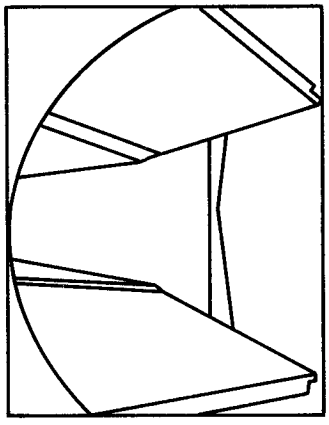

MACH NUMBER	0.8
ALTITUDE	7.315 M (24 000 FT)
NOZZLE VECTOR ANGLE	9 DEG

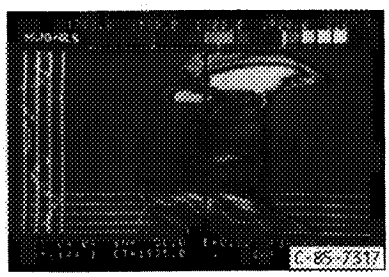

(A) VISUAL IMAGE. (B) INFRARED IMAGE.

FIGURE 27. - TYPICAL INFRARED IMAGE AT MAXIMUM AFTERBURNING CONDITION; VIEW FROM CAMERA PORT #3.

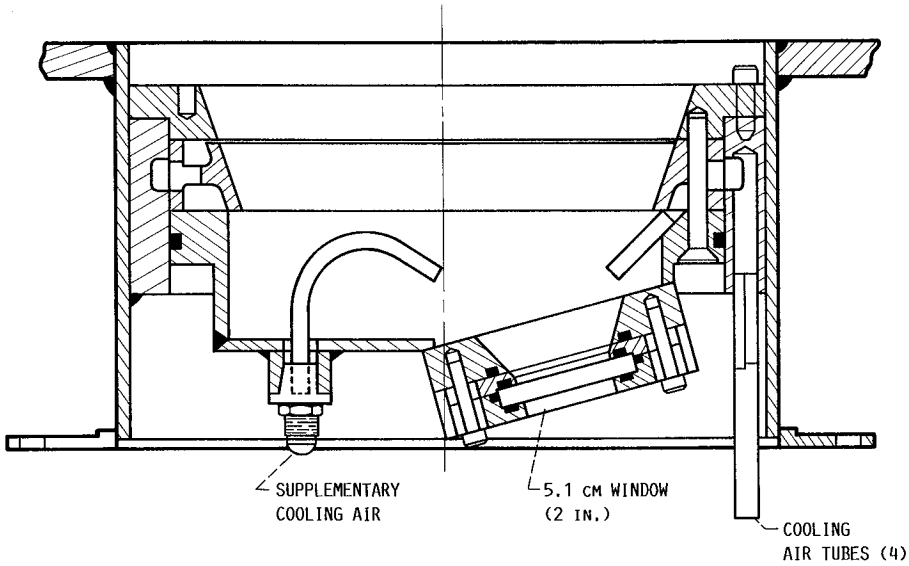

FIGURE 28. - SMALL WINDOW ASSEMBLY ADAPTATION.

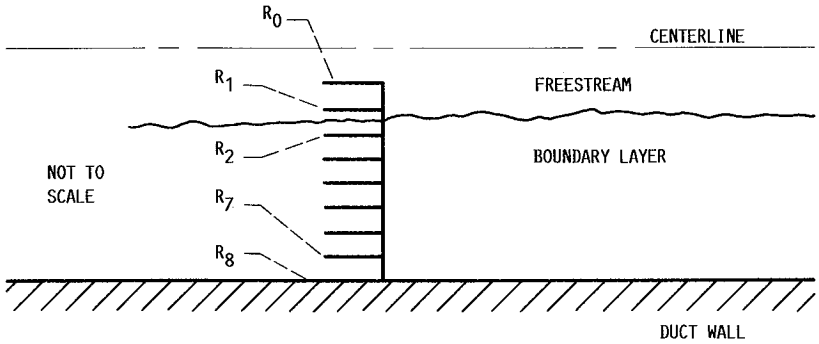

FIGURE A1. - STATION 1 TYPICAL BOUNDARY LAYER RAKE IMMERSIONS.

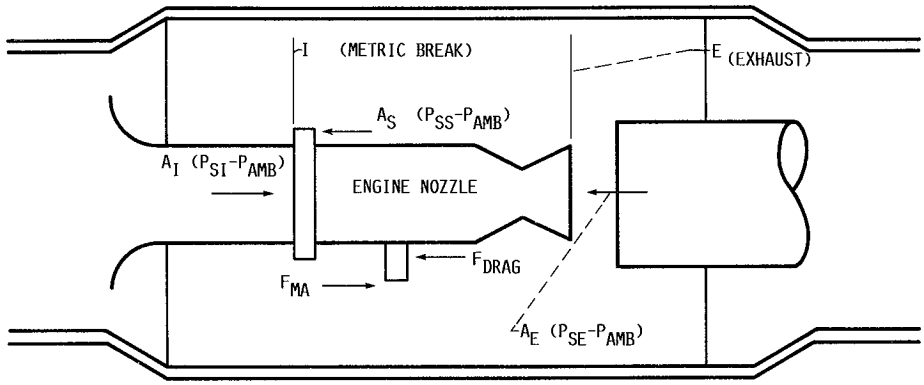

(A) AXIAL FORCES.

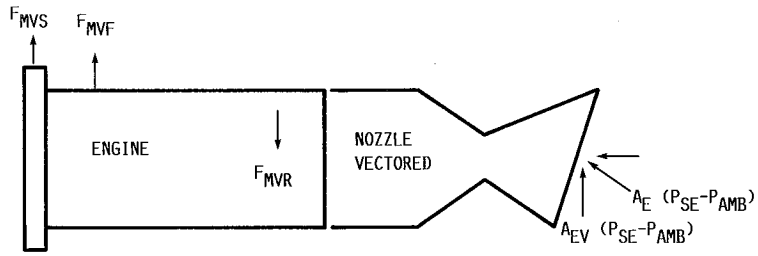

(B) VERTICAL FORCES.

FIGURE B1. - FORCES ACTING ON THE ENGINE AND NOZZLE.

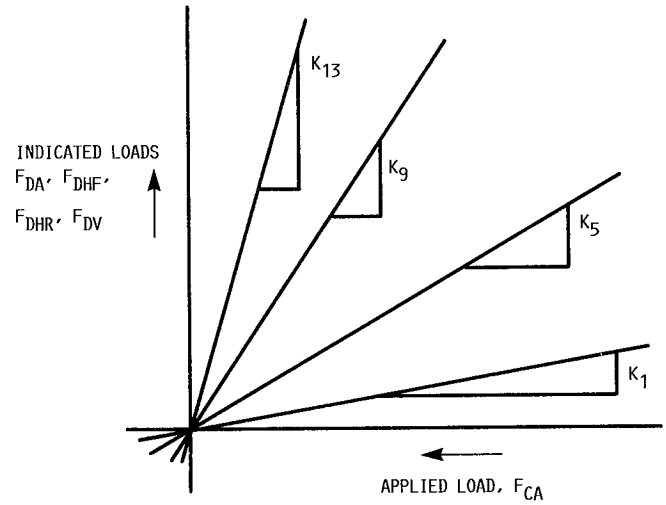

FIGURE B2. - GRAPHICAL REPRESENTATION OF K COEFFICIENTS.

NASA
National Aeronautics and Space Administration

Report Documentation Page

1. Report No.	2. Government Accession No.	3. Recipient's Catalog No.
NASA TM-100872		

4. Title and Subtitle
Techniques Utilized in the Simulated Altitude Testing of a 2D-CD Vectoring and Reversing Nozzle

5. Report Date
June 1988

6. Performing Organization Code

7. Author(s)
H. Bruce Block, Lively Bryant, John H. Dicus, Allan S. Moore, Maureen E. Burns, Robert F. Solomon, and Irving Sheer

8. Performing Organization Report No.
E-4096

10. Work Unit No.
505-62-3B

9. Performing Organization Name and Address
National Aeronautics and Space Administration
Lewis Research Center
Cleveland, Ohio 44135-3191

11. Contract or Grant No.

13. Type of Report and Period Covered
Technical Memorandum

12. Sponsoring Agency Name and Address
National Aeronautics and Space Administration
Washington, D.C. 20546-0001

14. Sponsoring Agency Code

15. Supplementary Notes
Irving Sheer, Retired.

16. Abstract

Simulated altitude testing of a two-dimensional, convergent-divergent, thrust vectoring and reversing exhaust nozzle was accomplished. An important objective of this test was to develop test hardware and techniques to properly operate a vectoring and reversing nozzle within the confines of an altitude test facility. This report presents detailed information on the major test support systems utilized, the operational performance of the systems and the problems encountered, and test equipment improvements recommended for future tests. The most challenging support systems included the multi-axis thrust measurement system, vectored and reverse exhaust gas collection systems, and infrared temperature measurement systems used to evaluate and monitor the nozzle. The feasibility of testing a vectoring and reversing nozzle of this type in an altitude chamber was successfully demonstrated. Supporting systems performed as required. During reverser operation, engine exhaust gases were successfully captured and turned downstream. However, a small amount of exhaust gas spilled out the collector ducts' inlet openings when the reverser was opened more than 60 percent. The spillage did not affect engine or nozzle performance. The three infrared systems which viewed the nozzle through the exhaust collection system worked remarkably well considering the harsh environment.

17. Key Words (Suggested by Author(s))	18. Distribution Statement
Jet engine testing; Altitude testing; 2D nozzles; Vectoring and reversing nozzles; Engine exhaust gas collection	Unclassified - Unlimited Subject Category 09

19. Security Classif. (of this report)	20. Security Classif. (of this page)	21. No of pages	22. Price*
Unclassified	Unclassified	42	A03

*For sale by the National Technical Information Service, Springfield, Virginia 22161